Angiogenesis (2022) 25:471–492
https://doi.org/10.1007/s10456-022-09840-x

ORIGINAL PAPER

TFEB controls integrin-mediated endothelial cell adhesion by the regulation of cholesterol metabolism

Camilla Ariano[1,2] · Chiara Riganti[3] · Davide Corà[4,5] · Donatella Valdembri[1,2] · Giulia Mana[1,2] · Elena Astanina[1,2] · Guido Serini[1,2] · Federico Bussolino[1,2] · Gabriella Doronzo[1,2]

Received: 15 November 2021 / Accepted: 18 April 2022 / Published online: 11 May 2022

Abstract

The dynamic integrin-mediated adhesion of endothelial cells (ECs) to the surrounding ECM is fundamental for angiogenesis both in physiological and pathological conditions, such as embryonic development and cancer progression. The dynamics of EC-to-ECM adhesions relies on the regulation of the conformational activation and trafficking of integrins. Here, we reveal that oncogenic transcription factor EB (TFEB), a known regulator of lysosomal biogenesis and metabolism, also controls a transcriptional program that influences the turnover of ECM adhesions in ECs by regulating cholesterol metabolism. We show that TFEB favors ECM adhesion turnover by promoting the transcription of genes that drive the synthesis of cholesterol, which promotes the aggregation of caveolin-1, and the caveolin-dependent endocytosis of integrin β1. These findings suggest that TFEB might represent a novel target for the pharmacological control of pathological angiogenesis and bring new insights in the mechanism sustaining TFEB control of endocytosis.

Keywords TFEB · Endothelial cells · Cell adhesion · Integrin · Cholesterol

Introduction

The plasma membrane of endothelial cells (ECs) is a very dynamic structure characterized by the presence of different adhesion receptors that regulate interconnected signaling pathways leading to blood vessel development and angiogenic remodeling [1, 2]. Among these receptors, integrins are αβ heterodimeric transmembrane protein dimers connecting the extracellular matrix (ECM) to the actin cytoskeleton and playing strategic roles during physiological and pathological angiogenesis [3, 4]. In ECs, integrins containing the β1 subunit are major ECM receptors that control cell adhesion, motility, proliferation and apoptosis [3, 4]. On the surface of ECs, integrins exist in a dynamic equilibrium between a bent/closed (inactive) and an extended/open (active) conformation, which exhibit low and high affinity for ECM ligands, respectively [5, 6].

The dynamics of ECM adhesions and the modulation of their strength depend not only on the conformational activation of integrins, but also on their localization in specific plasma membrane microdomains and endo-exocytic trafficking [6]. Depending on their subunit composition and ligand specificity, integrins can be internalized through clathrin-dependent or clathrin-independent pathways [6]. Caveolae are abundant surface pits formed by the assembly of cytoplasmic proteins on a platform generated by the plasma membrane embedded proteins caveolin-1 (CAV-1) and cavin and by membrane lipids [7]. The sequestration of high amounts of cholesterol is essential for caveolae formation, stability, and function [7]. Indeed, cholesterol is necessary for the aggregation of 8S CAV-1 oligomers into 70S CAV-1 multimers and for the insertion of hydrophobic central and

Federico Bussolino and Gabriella Doronzo have contributed equally to this work.

✉ Federico Bussolino
federico.bussolino@unito.it

✉ Gabriella Doronzo
gabriella.doronzo@unito.it

1 Department of Oncology, University of Torino, Candiolo, Italy

2 Candiolo Cancer Institute- FPO-IRCCS, Candiolo, Italy

3 Department of Oncology, University of Torino, Torino, Italy

4 Department of Translational Medicine, Piemonte Orientale University, Novara, Italy

5 Center for Translational Research on Autoimmune and Allergic Diseases—CAAD, Novara, Italy

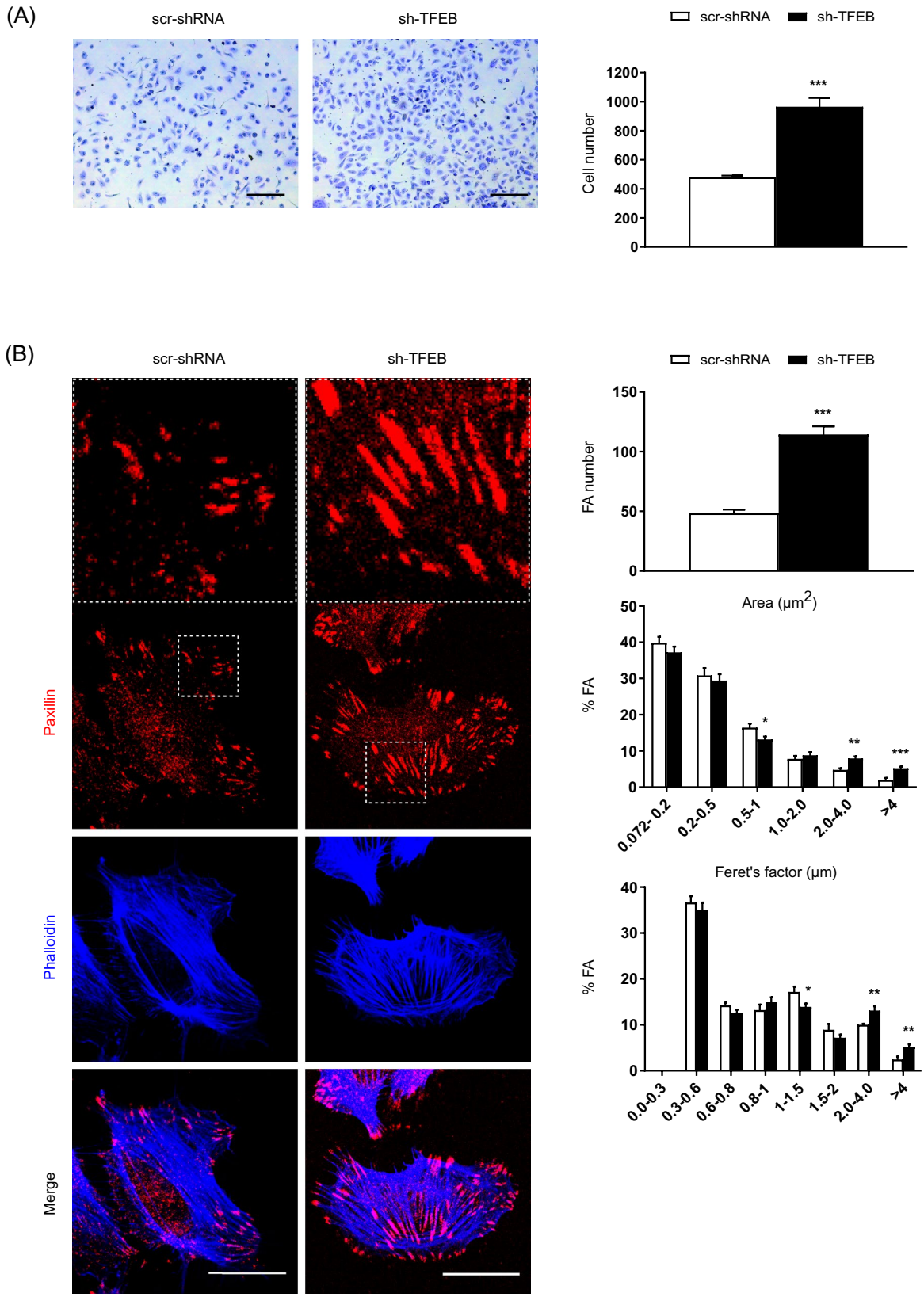
(A)
scr-shRNA
sh-TFEB
scr-shRNA
sh-TFEB
Cell number
1200
1000
800
600
400
200
0
***
(B)
scr-shRNA
sh-TFEB
Paxillin
Phalloidin
Merge
scr-shRNA
sh-TFEB
FA number
150
100
50
0
***
Area (μm2)
% FA
50
40
30
20
10
0
*
**
***
0.072- 0.2
0.2-0.5
0.5-1
1.0-2.0
2.0-4.0
>4
Feret's factor (μm)
% FA
40
30
20
10
0
*
**
**
0.0-0.3
0.3-0.6
0.6-0.8
0.8-1
1-1.5
1.5-2
2.0-4.0
>4

◂**Fig. 1** Modulation of FAs and adhesion by the silencing of physiological TFEB. **A** Representative images of adherent scr-shRNA- and sh-TFEB-ECs seeded on FN (10 × magnification, scale bar: 200 µm). The numbers of adherent cells are plotted as the mean ± SEM ($n = 3$ independent experiments; ***$p < 0.0001$ for sh-TFEB-ECs *versus* scr-shRNA-ECs, as determined by Student's *t* test). **B** Confocal microscopy analysis of scr-shRNA- and sh-TFEB-ECs stained with anti-paxillin Ab and phalloidin-647 (scale bar: 25 µm). The bar graphs show the quantification of the FA number, the FA area distribution (as the % of FAs with a definite area range *versus* the total number of FAs for each cell) and the Feret's diameter distribution (as the % of FAs characterized with a definite range of Feret's diameter *versus* the total number of FAs for each cell) ($n = 20$ cells per condition pooled from three independent experiments; values as mean ± SEM; ***$p < 0.0001$, **$p < 0.001$, and *$p < 0.01$ for sh-TFEB-ECs *versus* scr-shRNA-ECs, as determined by Student's *t* test)

C-terminal palmitoylated regions of CAV-1, within the plasma membrane [8]. Reducing cholesterol disrupts the integrity of caveolae, which results in its collapse into the plane of the plasma membrane and an uneven diffusion of CAV-1 [9, 10]. β1 subunit-containing integrins undergo caveolar endocytosis after binding to different ligands, including fibronectin, type I collagen, and glycosphingolipids [11]. In ECs, loss-of-function strategies targeting CAV-1 result in changes in the cellular shape, impairment of β1 integrin endocytosis, cell cycle G1/S phase transition, migration, and angiogenesis [12, 13]. Furthermore, in ECs, cholesterol regulates focal adhesion (FA) formation [14] and the organization of the actin cytoskeleton [15].

Transcription factor EB (TFEB), which was originally described as an oncogene involved in the onset of a subset of juvenile renal carcinomas [16], plays a major role as a regulator of lysosome biogenesis, autophagy, and metabolism [16–22]. This molecule is characterized by a basic helix-loop-helix leucine zipper structure, and its binding to DNA is mediated by an E-box nucleotide motif (GTCACG TGAC) named the "coordinated lysosomal expression and regulation" (CLEAR) motif [19, 20]. Under nutrient-rich conditions, TFEB is cytosolic and largely inactive, and the mTORC1-mediated phosphorylation of TFEB Ser142 and 211 serves as a docking site for chaperone 14-3-3, which sequesters it in an inactive state in the cytosol and favors its degradation. When cells sense nutrient deficiency and mTORC1 is inactive, TFEB moves to the nucleus, where it binds to the CLEAR motif in the promoter region of target genes [19–24]. We and others have revealed that TFEB is an important regulator of blood vessel formation and function [25–29]. Similar to its role in other cell types and organs [16–24], TFEB modulates genetic programs in vascular cells governing membrane traffic, lysosome biogenesis, autophagy, and exocytosis [25–29]. Furthermore, by coordinating the expression of genes involved in the control of the cell cycle and the trafficking of VEGF receptor 2 (VEGFR2), TFEB regulates EC proliferation [25]. Indeed, we previously showed that TFEB silencing leads to VEGFR2 accumulation at the plasma membrane, which is due to the impairment of its endocytosis through CAV-1-rich membrane rafts, a mechanism known to tune the signaling activities of VEGFR2 [30, 31], and its reduced degradation via the lysosomal autophagic pathway.

Here, we identify a novel function of TFEB that controls EC adhesion to the ECM by regulating the formation and turnover of adhesion sites via the expression of genes sustaining a metabolic program. By promoting the expression of genes involved in cholesterol synthesis and modulating the CAV-1-mediated internalization of β1 integrins, TFEB plays a key role in the control FA dynamics in ECs.

Results

TFEB inhibits EC adhesion and FA formation

To understand the physiological role of TFEB in the regulation of EC adhesion, we exploited cells in which endogenous TFEB was silenced by specific sh-RNA (sh-TFEB-ECs) and compared them with ECs carrying a control short hairpin RNA (scr-shRNA-ECs) (Fig. S1 A and B). ECs were seeded on fibronectin (FN), a prototypic provisional ECM component that is crucial for the formation of new blood vessels [32] and the number of adherent cells was quantified (Fig. 1A and Fig. S1 C). The adhesion of sh-TFEB-ECs was increased compared with that of scr-shRNA-ECs (Fig. 1A and Fig. S1 C) thus suggesting that TFEB may modulate angiogenesis by influencing not only EC proliferation [25], but also EC adhesion to the ECM.

To directly investigate this hypothesis, we analyzed the pattern of F-actin and paxillin-labeled FAs in control and TFEB-silenced ECs plated on FN, by confocal fluorescence microscopy. As shown in Fig. 1B and Fig. S1 D, both sh-TFEB-ECs and scr-shRNA-ECs displayed typical elongated and thick actin stress fibers, and TFEB silencing resulted in the formation of more numerous and larger FAs, as evaluated by measuring the area and Feret's diameter (*i.e.,* the longest FA axis) (Fig. 1B and Fig. S1 D). Indeed, in TFEB-silenced ECs FA area and Feret's diameter were 60% and 50% higher than in control ECs, respectively (Average FA area: scr-shRNA-ECs 1.2 ± 0.04 µm^2 and sh-TFEB-ECs 1.9 ± 0.05 µm^2, $p = 0.005$; average Feret's diameter: scr-shRNA-ECs 1.4 ± 0.03 µm and sh-TFEB-ECs 2.1 ± 0.04 µm, $p = 0.003$; values as means ± SEMs; p as determined by Student's *t* test; $n = 20$ cells per condition pooled from 3 independent experiments) (Fig. 1B).

Hence, the observed increased adhesion of TFEB-silenced ECs to provisional ECM proteins might rely on defects in FA turnover and dynamics.

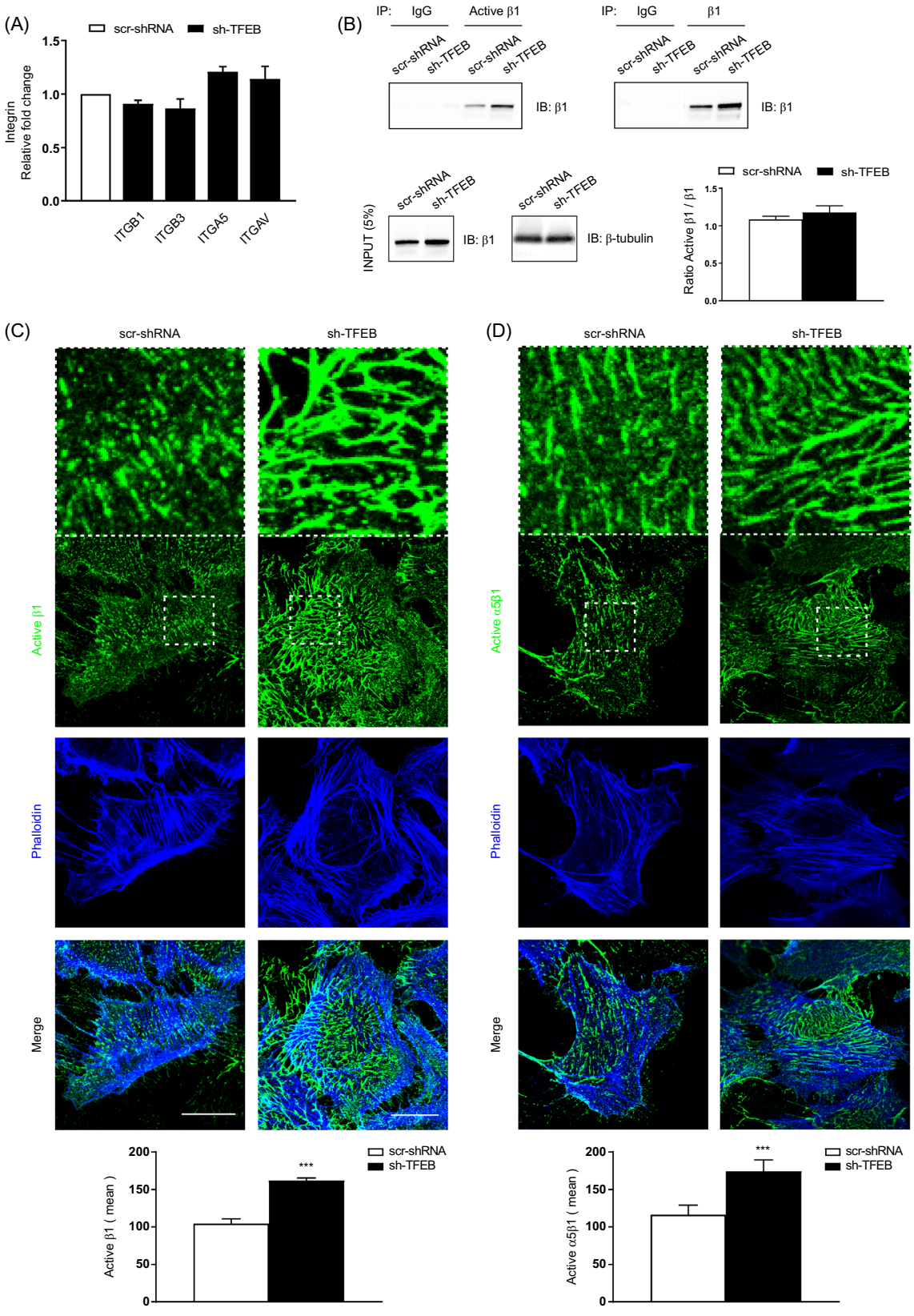
(A)
scr-shRNA
sh-TFEB
Integrin Relative fold change
1.5
1.0
0.5
0.0
ITGB1
ITGB3
ITGA5
ITGAV
(B)
IP: IgG
Active β1
IP: IgG
β1
scr-shRNA
sh-TFEB
scr-shRNA
sh-TFEB
IB: β1
IB: β1
INPUT (5%)
IB: β1
IB: β-tubulin
Ratio Active β1 / β1
(C)
scr-shRNA
sh-TFEB
Active β1
Phalloidin
Merge
Active β1 (mean)
200
150
100
50
0
***
(D)
scr-shRNA
sh-TFEB
Active α5β1
Phalloidin
Merge
Active α5β1 (mean)
200
150
100
50
0
***

◂**Fig. 2** TFEB silencing increases the integrin protein levels. **A** qPCR of *ITGB1, ITGB3, ITGA5 and ITGAV* expression in scr-shRNA and sh-TFEB-ECs. Data are expressed as relative fold change in sh-TFEB-ECs compared with the expression in scr-shRNA-ECs after normalization to the housekeeping gene *TBP* ($n=3$ independent experiments, values as mean ± SEM; p = ns sh-TFEB-ECs *versus* scr-shRNA-ECs by Student's t test). **B** Representative western blot of active and total β1 integrins immunoprecipitated from scr-shRNA- or sh-TFEB-ECs lysates. After immunoprecipitation (IP) with anti-active β1 integrin (9EG7) and anti-total β1 integrin antibodies, proteins were blotted (IB) with anti-total β1 integrin antibody. In the same lysates used for immunoprecipitation, the endogenous expression of total β1 integrin and β-tubulin were blotted with the specific antibodies and presented as "input". **C**, **D** Confocal microscopy analysis of plasma membrane active-β1 and active- α5β1 integrin expression and localization in living scr-shRNA- and sh-TFEB-ECs following incubation with anti-active β1 integrin (9EG7), active-α5β1 (SNAKA-51) and phalloidin-647 (scale bar: 25 µm). The bar graphs show the quantification of the mean intensity of active-β1 integrin and active- α5β1 ($n=10$ cells per condition pooled from three independent experiments; values as mean ± SEM; ***$p<0.0001$ sh-TFEB-ECs *versus* scr-shRNA-ECs, as determined by Student's t test)

TFEB silencing increases surface β1 integrins, fibrillar adhesions and fibronectin fibrillogenesis

Integrins are key ECM receptors and their endo-exocytic trafficking is crucial for the regulation of FA turnover and ECs adhesion [6]. In particular, α5β1 integrin recognizes FN as specific ECM ligand supporting its remodeling, internalization and degradation [32–34].

Although TFEB silencing in ECs did not modify the transcription of the major integrin subunit genes, such as *ITGA5*, *ITGAV*, *ITGB1* and *ITGB3* (Fig. 2A and Fig. S2 A), it increased the cellular amount of total and conformationally active β1 and active α5β1 integrin (Fig. S1 B, Fig. 2B and Fig. S2 B). The unchanged ratio between active/total β1 in sh-TFEB- compared to scr-shRNA-ECs suggested that the lack of TFEB increases total β1 integrin amounts, but not its activation (Fig. S1 B, Fig. 2B and Fig. S2 B). In addition, we evaluated the distribution of conformationally active β1 and α5β1 integrin at the plasma membrane. Confocal immunofluorescence microscopy showed that, compared to scr-shRNA-ECs, sh-TFEB-ECs were characterized by higher amount of active β1 and α5β1 integrin on the cell surface (Average fibrillar adhesion size: active $\beta1^+$: scr-shRNA-ECs 2.6 ± 0.6 µm; sh-TFEB-ECs 10.9 ± 2.0 µm; active $\alpha5\beta1^+$: scr-shRNA-ECs 3.8 ± 1.1 µm; sh-TFEB-ECs 12.3 ± 3.4 µm; values as mean ± SEM, $p<0.0001$ as determined by Student's t test; $n=10$ cells from 3 independent experiments) (Fig. 2C and D).

Compared to scr-shRNA-ECs, sh-TFEB-ECs displayed not only higher amount and size of FAs but also of fibrillar adhesions, as evidenced by the co-localization of active β1 integrin and the cytoskeletal adaptor tensin (Fig. S1 E).

As previously described [35–37], ECs are able to synthesize endogenous FN dimers that, upon binding to α5β1 integrin, polymerize into an extracellular fibrillary network [11, 34–39]. As expected, ECs physiologically synthesize endogenous FN (Fig. S2 C, Fig. S2 D and Fig. S2 E). Furthermore, TFEB silencing increased both FN quantity and its polymerization into fibrils (Fig. S2 C, Fig. S2 D and Fig. S2 E). Quantitative real time PCR (qPCR), showed that TFEB silencing did not modify FN mRNA level in ECs (Fig. S2 D), suggesting that the observed increase in FN protein level could be probably due to a posttranslational regulation, e.g., endocytosis and degradation.

Integrin-mediated adhesion to the ECM activates the autophosphorylation of focal adhesion kinase (FAK) and Src family kinases along with the recruitment of adaptor proteins [40–42]. We found that both FAK and Src proteins were more activated in sh-TFEB- vs scr-shRNA-ECs, as evidenced by the Western blot analysis of the pTyr397/total FAK and pTyr416/Total Src protein ratio (Fig. S2 F).

TFEB silencing inhibits β1 integrin internalization and degradation

Because we previously demonstrated that TFEB regulates the trafficking of transmembrane protein receptors [25], we wondered whether the increase of surface β1 integrins, fibrillar adhesions, and fibronectin fibrillogenesis observed in TFEB-silenced ECs could be due to alterations in β1 integrin internalization. Biochemical time course analyses showed that, compared to controls, TFEB silencing decreased the internalization of both total and active β1 and active α5β1 integrins (41.4 ± 7.7%, 45.0 ± 5.8%, 46.9 ± 8.1%, after 30 min, respectively; values as mean ± SEM, $p=0.001$ and $p=0.0003$, respectively as determined by Student's t-test; n = 3 independent experiments) (Fig. 3A and B). Of note, in sh-TFEB-ECs, the significantly reduced endocytic rate was paralleled by the simultaneous increase of both total and active β1 and active α5β1 integrin distribution at the cell surface (Fig. 3B).

Upon internalization, integrins are delivered to early endosomes and then either routed to lysosomes for degradation or recycled back to the plasma membrane [5, 6, 43–45]. TFEB regulates via CLEAR motif the transcription of genes encoding for vesicle membrane proteins, hydrolases and proteins involved in the regulation of endocytosis and exocytosis processes [18–29]. The lack of TFEB resulted in the reduction of LAMP-1^+ lysosomes (64.6 ± 6,.9%), but not $EEA1^+$ early endosomes (Fig. 3C) and, as evidenced in Fig. 3C and Fig. S3 A, total and active β1 and active α5β1 integrin amounts were significantly reduced in both early endosomes and lysosomes in agreement with the observed reduction of integrin internalization (Fig. 3A and B). Moreover, TFEB silencing resulted in the reduced degradation rate of internalized active β1 integrin (Fig. S3 B).

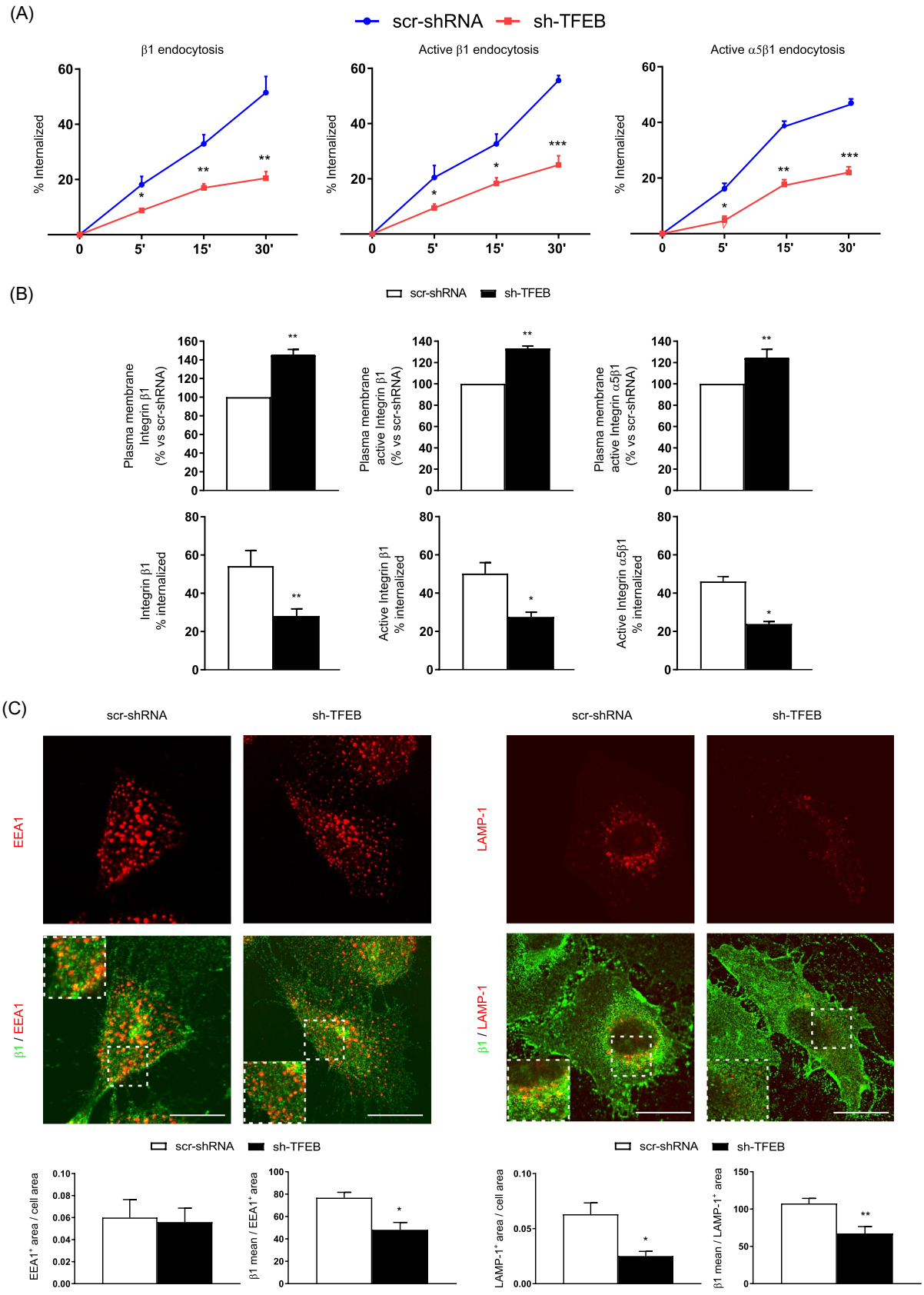
(A)
scr-shRNA
sh-TFEB
β1 endocytosis
Active β1 endocytosis
Active α5β1 endocytosis
% Internalized
0
5'
15'
30'
(B)
scr-shRNA
sh-TFEB
Plasma membrane Integrin β1 (% vs scr-shRNA)
Plasma membrane active Integrin β1 (% vs scr-shRNA)
Plasma membrane active Integrin α5β1 (% vs scr-shRNA)
Integrin β1 % internalized
Active Integrin β1 % internalized
Active Integrin α5β1 % internalized
(C)
scr-shRNA
sh-TFEB
EEA1
β1 / EEA1
LAMP-1
β1 / LAMP-1
EEA1+ area / cell area
β1 mean / EEA1+ area
LAMP-1+ area / cell area
β1 mean / LAMP-1+ area

◂**Fig. 3** TFEB silencing inhibits β1 integrin internalization. **A** Time-course analysis of the relative amounts of internalized total and active β1 and active- α5β1 integrin in scr-shRNA-ECs and sh-TFEB-ECs. Integrin internalization was evaluated by integrin internalization assay and capture ELISA assay ($n=3$ independent experiments, values as mean ± SEM, ***$p<0.0001$, **$p<0.001$, *$p<0.01$ all samples *versus* scr-shRNA-ECs as determined by Student's *t* test). **B** Analysis of the relative amounts of internalized total and active β1 and active-α5β1 integrin in scr-shRNA-ECs and sh-TFEB-ECs ($n=3$ independent experiments, values as mean ± SEM, **$p<0.001$, *$p<0.01$ all samples *versus* scr-shRNA-ECs by Student's *t* test). **C** Confocal microscopy analysis of total β1 integrin localization in $EEA1^+$ and $LAMP\text{-}1^+$ vesicles in scr-shRNA-ECs and sh-TFEB-ECs stained with anti-β1 integrin, anti-EEA1 and anti-LAMP-1 Abs (scale bar: 50 μm). Bar graph shows the quantification of $EEA1^+$ and $LAMP\text{-}1^+$ areas per cell area and the amount of β1 integrin accumulated in $EEA1^+$ and $LAMP\text{-}1^+$ areas ($n=20$ cells per condition pooled from three independent experiments, values are mean ± SEM; *$p<0.01$, **$p<0.001$ scr-shRNA- *versus* sh-TFEB-ECs as determined by Student's *t* test)

TFEB silencing reduces CAV-1 plasma membrane localization and caveolar β1 integrin internalization

CAV-1 participates in the regulation of β1 integrin endocytosis [7]. We previously revealed that the silencing of TFEB in ECs dysregulates the interplay between CAV-1 and VEGFR2 [25]. Hence, we posited that the decreased β1 integrin internalization observed in sh-TFEB-ECs could be due to alterations in CAV-1-dependent internalization and trafficking. In ECs, TFEB silencing did not change *CAV-1* gene transcription (The relative fold change in sh-TFEB-ECs compared with the expression in scr-shRNA-ECs after normalization to the housekeeping gene *TBP* was 0.9 ± 0.1; value as mean ± SEM; $p=$ ns as determined by Student's *t* test; $n=3$ independent experiments) and cellular protein levels compared to control cells (Fig. 4A). However, total internal reflection fluorescence (TIRF) microscopy analysis of the EC surface showed a reduction of CAV-1 at plasma membrane (Fig. 4B) and a decreased proximity between CAV-1 and active β1 integrin (Fig. 4B) in sh-TFEB-ECs respect of scr-shRNA-ECs. Stimulated emission depletion (STED) confocal fluorescence microscopy analysis and 3D-STED super-resolution imaging revealed that CAV-1 and active β1 integrin were in close proximity and co-internalized in scr-shRNA-ECs but not in sh-TFEB-ECs (Fig. 5A).

TFEB modulates integrin internalization through cholesterol homeostasis

To further analyze the role of TFEB in CAV-1-mediated β1 integrin endocytosis, we subsequently assessed whether TFEB could regulate the homeostasis of cholesterol, which is instrumental in CAV-1 patterning at the plasma membrane [7–15]. Biochemical analysis of ECs demonstrated a clear reduction in the total cellular cholesterol quantity after TFEB silencing (Fig. 5B). In scr-shRNA- and sh-TFEB-ECs we also quantified the amounts of membrane-free and unesterified cholesterol, which is mainly contained in the plasma membrane [46], and esterified cholesterol, which is typically contained in cytosolic stores. Interestingly, the loss of TFEB reduced free and esters cholesterol per se (Fig. 5B), but it did not modify the ratio between free/total cholesterol and esters/total cholesterol (Fig. 5C), suggesting a defect in cholesterol synthesis, but not an alteration of its subcellular distribution.

The synthesis of cholesterol and cholesterol intermediates and side products, such as the isoprenoids farnesyl pyrophosphate (FPP), geranylgeranyl pyrophosphate (GGPP) and the isoprenoid-containing molecule ubiquinone, was clearly reduced in sh-TFEB-ECs, compared with scr-shRNA-ECs (Fig. 6A). In contrast, the lack of TFEB did not affect cholesterol uptake and efflux (Cholesterol uptake: sh-TFEB-ECs as % of scr-shRNA-ECs 101.1 ± 10.1; cholesterol efflux: sh-TFEB-ECs as % of scr-shRNA-ECs 96.7 ± 6.7; values as mean ± SEM, $p=$ ns as determined by Student's *t* test; $n=3$ independent experiments).

The biosynthesis of cholesterol is regulated by different enzymes and the endoplasmic reticulum (ER) transmembrane protein complex sterol-regulatory element-binding protein-2 (SREBP-2, *SREBF-2*)/SREBP cleavage-activating protein (SCAP) [46]. The N-terminal domain of membrane-associated SREBP-2 displays a basic helix-loop-helix (bHLH) folding. Upon SCAP-mediated trafficking from the ER to the Golgi, SREBP-2 is cleaved by proteases to release its bHLH in the cytosol that is then translocated into the nucleus to act as a transcription factor. The bHLH domain of SREBP2 induces the transcription of key genes involved in cholesterol metabolism, including β-Hydroxy β-methylglutaryl-CoA reductase (HMGCR), the rate limiting enzyme of cholesterol synthesis [46].

Remarkably, we found that TFEB silencing inhibited the transcription of the *SREBF-2* and *SCAP* genes and the SREBP-2 target gene *HMGCR* (Fig. 6B). Furthermore, as evidenced by confocal fluorescence microscopy and immunoblot analysis (Fig. 6C and D), and consistent with the significant decrease in the biosynthesis of cholesterol and its intermediates (Fig. 6A), the levels of SCAP protein, HMGCR protein (Fig. 6C), unprocessed SREBP-2 precursor protein, and cleaved mature N-terminal bHLH domain of SREBP-2 (Fig. 6D) were significantly reduced in sh-TFEB-ECs. After TFEB silencing HMGCR expression and cholesterol synthesis were similar to that observed after HMGCR silencing in scr-shRNA-ECs, suggesting that indeed TFEB may act by promoting the transcription of *HMGCR* (Fig. S4 A). Even after HMGCR silencing in scr-shRNA-ECs the ratio between free/total cholesterol and cholesteryl esters/total cholesterol were unchanged (Fig. S4 A).

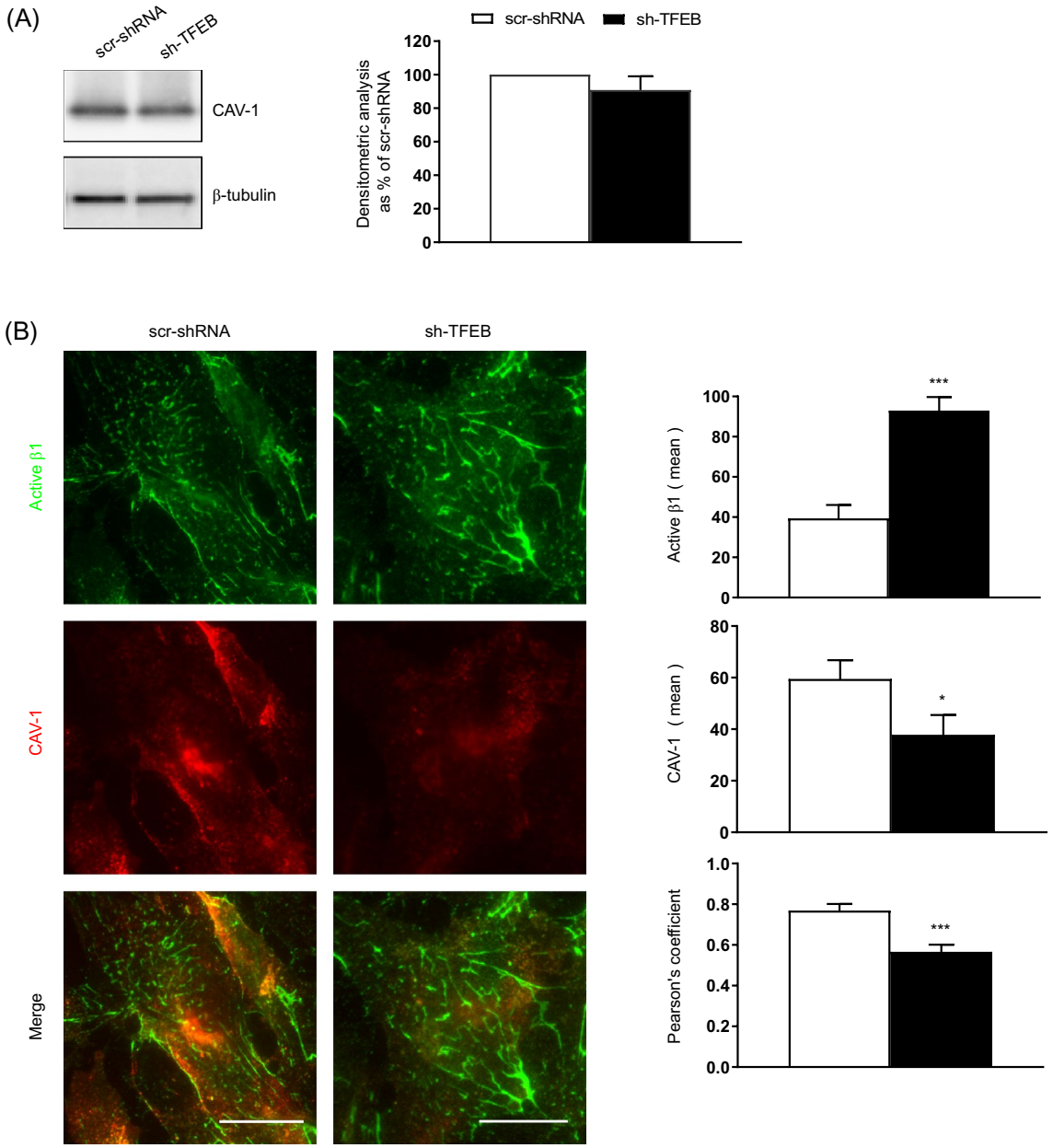

Fig. 4 TFEB silencing inhibits CAV-1 membrane distribution and integrin/CAV-1 proximity. **A** Representative western blots of cellular amount of CAV-1 expression in scr-shRNA- and sh-TFEB-ECs. Bar graph shows the densitometric analysis expressed as the ratio between CAV-1 and β-tubulin ($n=3$ independent experiments, values as mean ± SEM; $p=$ ns sh-TFEB- *versus* scr-shRNA-ECs by Student's *t* test). **B** Representative TIRF images of active β1 integrin and CAV-1 in living scr-shRNA- and sh-TFEB-ECs. After in vivo incubation with anti-active β1 integrin (9EG7) antibody, cells were stained with anti-CAV-1 antibody (scale bar: 25 μm). The bar graphs show the quantification of the mean intensity of active β1 integrin and CAV-1 and the proximity of the two proteins analyzed with Pearson's coefficient ($n=20$ cells per condition pooled from three independent experiments; values as mean ± SEM; $^{***}p<0.0001$ and $^{*}p<0.01$ for sh-TFEB-ECs *versus* scr-shRNA-ECs, as determined by Student's *t* test)

Altogether, these data suggest that in ECs lacking TFEB the surface accumulation of β1 integrins and the ensuing enlargement and stabilization of FAs may be due to the reduction of plasma membrane-free cholesterol, CAV-1 clustering, and caveolae-mediated β1 integrin internalization [10–15].

To validate these assumptions, we performed experiments in which cholesterol amounts were modulated (Figs. 7, 8, 9 and Fig. S4 C-D). In particular, we depleted endogenous cholesterol by treating scr-shRNA- and sh-TFEB-ECs with β-methyl cyclodextrin (βMCD) (5 mM, 1 h). Similarly to what observed in sh-TFEB-ECs, the depletion of endogenous

cholesterol in scr-shRNA- ECs reduced the internalization of both total and active β1 integrin (Fig. S4 B). Moreover, cholesterol depletion in scr-shRNA-ECs increased both total and active β1 integrin amounts albeit to a lesser extent than in sh-TFEB ECs (Fig. S4 C). As expected, treatment of scr-shRNA-ECs with the specific inhibitor of lysosome activity, the vacuolar H^+ ATPase inhibitor bafilomycin A1 [47] also due to the increase of total and active β1 integrins amount (Fig. S4 C) but only the contemporary presence of bafilomycin A1 and cholesterol depletion mimicked the effect on total and active β1 integrin observed in sh-TFEB-ECs (Fig. S4 C).

On the contrary, we tried to rescue sh-TFEB-ECs phenotype by ECs treatment with exogenous cholesterol. Upon depletion of endogenous cholesterol by βMCD (5 mM, 1 h) and treatment with different concentrations of exogenous cholesterol (1–30 µg/ml, 24 h), we found that the minimal concentration of exogenous cholesterol capable of restoring in sh-TFEB-ECs total cellular cholesterol levels comparable to those of scr-shRNA-ECs was 5 µg/ml, a concentration that we hence employed in rescue experiments (Fig. S4 D and Figs. 7, 8, 9). In sh-TFEB-ECs the normalization of total cholesterol quantity led to the rescue of free cholesterol level (Fig. S4 D). Free/total and cholesteryl esters/total cholesterol ratios were similar after adding 5 µg/ml of exogenous cholesterol in the two cell types (Ratio free / total cholesterol: scr-shRNA-ECs + cholesterol 0.14 ± 0.01; sh-TFEB-ECs + cholesterol 0.13 ± 0.1; ratio cholesteryl esters / total cholesterol: scr-shRNA-ECs + cholesterol 0.08 ± 0.01; sh-TFEB-ECs + cholesterol 0.09 ± 0.01; values as mean ± SEM, p = ns as determined by Student's t test; $n = 3$ independent experiments). Of note, the addition of exogenous cholesterol in sh-TFEB-ECs restored total and active β1 integrin surface amounts (Fig. 7A and Fig. S5 A) and internalization rates (Fig. 7A) similar to those of scr-shRNA-ECs and substantially, yet not completely, rescued total and active β1 integrin levels (Fig. S4 C), probably because integrin degradation was still blocked (Fig. 3 C, Fig. S3 A and B).

Similarly, TIRF and STED microscopy evidenced that the addition of exogenous cholesterol on sh-TFEB-ECs normalized the distribution of CAV-1 at the plasma membrane, and reestablished the proximity between CAV-1 and active β1 integrin (Fig. 7B and Fig. 8) along with CAV-1-mediated internalization of active β1 integrins (Fig. 8).

Consistently, the addition of exogenous cholesterol rescued abnormal phenotypes observed in sh-TFEB-ECs such as FA average number, size and diameter (Fig. 9A) as well as fibrillar adhesions number and length (Fig. S5 B)(scr-shRNA-ECs + cholesterol: $n = 158.4 \pm 15.4$ and average size 0.43 ± 0.04 µm; sh-TFEB-ECs + cholesterol: $n = 172.1 \pm 8$ and average size 0.48 ± 0.07 µm; values as means ± SEMs; p = ns as determined by Student's t test; $n = 10$ cells per condition pooled from 3 independent experiments) and cell adhesion (Fig. 9B).

Discussion

In this study, we unveil a novel function of TFEB as a transcriptional regulator of metabolic signaling pathways that control integrin-mediated EC adhesion to the ECM. We reveal that TFEB is involved in the control of cholesterol synthesis via the transcriptional modulation of genes encoding the sterol sensor SCAP and the associated transcription factor and key regulator of cholesterol homeostasis SREBP-2. TFEB-silenced ECs show defects in endogenous cholesterol synthesis and are characterized by inhibition of the cholesterol-dependent clustering of plasma membrane CAV-1, the association β1 integrin with CAV-1 and their internalization. In particular, after TFEB silencing the integrin increased level is mediated by the block of integrin internalization and degradation as the result of the inhibition of cholesterol synthesis, altered distribution of cholesterol on plasma membrane and reduced lysosome-dependent protein degradation.

TFEB is emerging as a key modulator of cellular metabolism, including triglyceride and fatty acid catabolism [48]. Here, we discover that TFEB also promotes endogenous cholesterol synthesis in ECs. Cells sense the endogenous cholesterol levels through the regulatory protein SCAP, which associates with the master regulator of cholesterol biosynthesis SREBP-2 [46]. Cholesterol binding to the sterol-sensing domain of SCAP stabilizes the association of the SCAP/SREBP2 complex with the ER resident protein Insulin Induced Gene 1 (INSIG1). In contrast, in the presence of low endogenous cholesterol levels, the SCAP/SREBP2 complex disconnects from INSIG1 and relocates to the Golgi, where proteases cleave and free the bHLH domain of SREBP2 in the cytosol [46]. The active form of SREBP2 then moves to the nucleus and induces the transcription of cholesterol metabolism genes [46]. Similarly in other cell types [49], TFEB is also able to modulate cholesterol synthesis in ECs. We found that a lack of TFEB resulted in the transcriptional down-regulation of SCAP, SREBP2 and HMGCR. TFEB did not affect cholesterol uptake or efflux, which are two events that might dynamically regulate the amount of intracellular cholesterol, and these findings suggest that reductions in endogenous synthesis might reduce the amount of plasma membrane-associated cholesterol.

Different studies unveiled a cross-talk between the nutrient cellular status and the trafficking of integrins [50–53]. In particular, in cancer cells mTOR inhibition due to nutrient depletion promotes the tensin-dependent maturation of subnuclear fibrillar adhesions and the ensuing localized endocytosis of fibronectin-bound active α5β1 integrin [51]. Probably because of the lysosomal degradation of fibronectin and the increased availability of amino acids, the internalization of fibronectin-bound active α5β1 integrin activates mTOR,

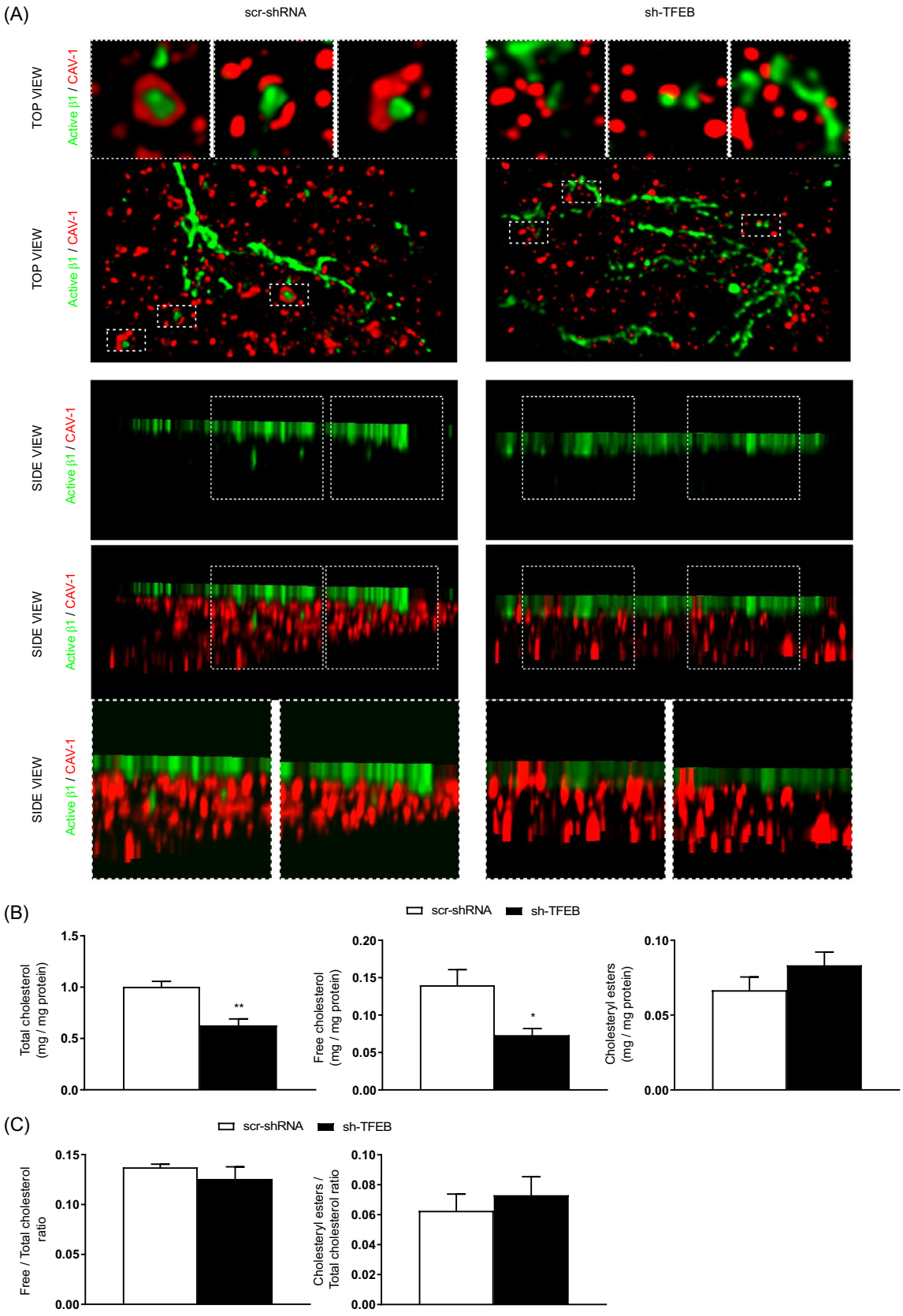
(A)
scr-shRNA
sh-TFEB
TOP VIEW
Active β1 / CAV-1
SIDE VIEW
(B)
scr-shRNA
sh-TFEB
Total cholesterol (mg / mg protein)
Free cholesterol (mg / mg protein)
Cholesteryl esters (mg / mg protein)
(C)
Free / Total cholesterol ratio
Cholesteryl esters / Total cholesterol ratio

◂**Fig. 5** TFEB silencing reduces integrin/CAV-1 proximity and integrin internalization via cholesterol synthesis inhibition. **A** Representative 3D-STED super-resolution image of total/ active β1 integrin and CAV-1 expression and localization in living scr-shRNA- and sh-TFEB-ECs. After in vivo incubation with anti-active β1 integrin (9EG7) antibody, cells were stained with CAV-1 antibody (scale bar: 0.5 μm; $n = 5$ cells per condition pooled from three independent experiments). **B** The bar graphs show the quantification of total cholesterol, free cholesterol and cholesteryl esters in scr-shRNA- and sh-TFEB-ECs ($n = 3$ independent experiments; values as mean ± SEM; $^{**}p < 0.001$ and $^{*}p < 0.01$ for sh-TFEB-ECs *versus* scr-shRNA-ECs, as determined by Student's *t* test). **C**The bar graphs show the ratio between free and total cholesterol and cholesteryl esters and total cholesterol in scr-shRNA- and sh-TFEB-ECs ($n = 3$ independent experiments; values as mean ± SEM; p = ns for sh-TFEB-ECs *versus* scr-shRNA-ECs, as determined by Student's *t* test)

which in turn impairs the maturation of sub-nuclear fibrillar adhesions [33].

In addition, nutrient and energy sensing crucially relies on AMP-activated protein kinase (AMPK), which is activated by reduced nutrients or increased AMP/ATP ratio [50–54]. Of note, in wild type fibroblasts activated AMPK inhibits the transcription of tensin and in AMPK knockout fibroblasts tensin silencing impairs the activation of α5β1 integrin, cell spreading, traction stress, and fibronectin fibrillogenesis [51, 52].

Nutrient cellular status and mTORC1 activity are strongly involved in TFEB phosphorylation and nuclear translocation [18, 21, 22]. Some studies described an AMPK-mediated activation of TFEB that was abolished in AMPK null models probably via mTORC1 in some cellular conditions [55–57]. Along this line, it is tempting to speculate that the reported inhibitory activity of AMPK on α5β1 integrin function [50–52] may be mediated at least in part by the TFEB-mediated activation of cholesterol and CAV-1-driven β1 integrin endocytosis.

The formation and remodeling of FAs depend on conformational activation, endo-exocytic trafficking and degradation of integrin [5–9, 11–13]. From the plasma membrane, integrins are internalized, *e.g.,* in a clathrin- or caveolin-dependent manner, and then, through endosomal sorting, these molecules are recycled back to the cell surface or degraded in lysosomes [5–9, 11–13].

Caveolae and lipid rafts are specific plasma membrane structures composed by cholesterol, glycosphingolipids, and CAV-1, involved in endocytosis, protein trafficking, and signaling. CAV-1 tightly binds to cholesterol, and both molecules are necessary for the formation of caveolar invaginations and cholesterol-promoting CAV-1 multimerization [7–10]. Various studies have indicated that CAV-1 and cholesterol are key molecules in the regulation of ECs adhesion and migration on FN during angiogenesis [12, 13, 58–62].

Alteration of cholesterol plasma membrane amounts results in the inhibition of key regulators of ECs proliferation such as mTOR and VEGFR2 [59, 61–63]. Reduction of cholesterol trafficking correlates with the inhibition of mTOR activation as a consequence of its translocation on perinuclear lysosomes [61]. Furthermore, in vascular cells cholesterol regulates the receptor membrane topology and activities of VEGFR2, PDGFRβ and Endothelial Activin receptor-like kinase-1 [61–64]. We previously described that endothelial TFEB silencing leads to an anti-angiogenic phenotype supported by VEGFR2 mis-localization at plasma membrane as a consequence of post-transcriptional regulation, de-localization in non-caveolar areas and inhibition of its internalization [25].

Our findings extended the role of TFEB in regulating the functions of membrane receptors and integrins. We propose that under physiological conditions, TFEB participates in integrin traffic by regulating cholesterol bioavailability and CAV-1 subcellular distribution. Indeed, in TFEB-silenced ECs, the plasma membrane patterning of CAV-1, but not its protein levels, was abnormally altered. After TFEB silencing, similarly to previously described via loss-of-function strategies targeting CAV-1 we evidenced an impairment of β1 integrin endocytosis [12, 13]. Furthermore, in ECs, cholesterol regulates FA formation [14] and the organization of the actin cytoskeleton [15].

Endocytosis and degradation or recycling from different vesicular compartments determine the fate of integrins [5, 6, 11, 42–45, 65–72]. In particular, via different mechanisms, active α5β1 integrin after caveolin and clathrin-endocytosis is in part recycled at PM and in part degraded in lysosomes [5, 6, 11, 42–45, 65–72]. FN binding triggers the ubiquitination and the internalization of α5β1 integrin [66]. Most FN-bound α5β1 is de-ubiquitinated and, after FN dissociation, recycled back to plasma membrane [67]. The residual ubiquitinated α5β1 integrin traffics to multivesicular bodies (MVBs) and then to lysosomes where it undergoes degradation [66, 67]. After overexpression of Rab25, endocytosed active α5β1 integrin is also delivered to MVBs from which it recycles back to plasma membrane [68]. Sorting nexin (SNX)-17 binds β1 integrins to prevent their lysosomal degradation and to favor their recycling from endosome to plasma membrane [44, 45]. There are also evidence that internalized FN is actually recycled/secreted from late endosomes and lysosomes [69] and that the endocytosis of FN-bound active α5β1 integrin is sustained by Rab21 [70].

Of note, in ECs was previously described that upon internalization, the FN/active α5β1 integrin complex moves to post Golgi carrier vesicles (PGCs) where α5β1 integrins detach from FN fragments, associates with freshly synthesized FN dimers, and reaches the basolateral side of the plasma membrane [36]. More recently, in endothelium the CDC42-related RHO-family member RHOJ was found to inhibit the accumulation of endocytosed FN-bound/active α5β1 integrins in early endosomes, their transport to PGCs

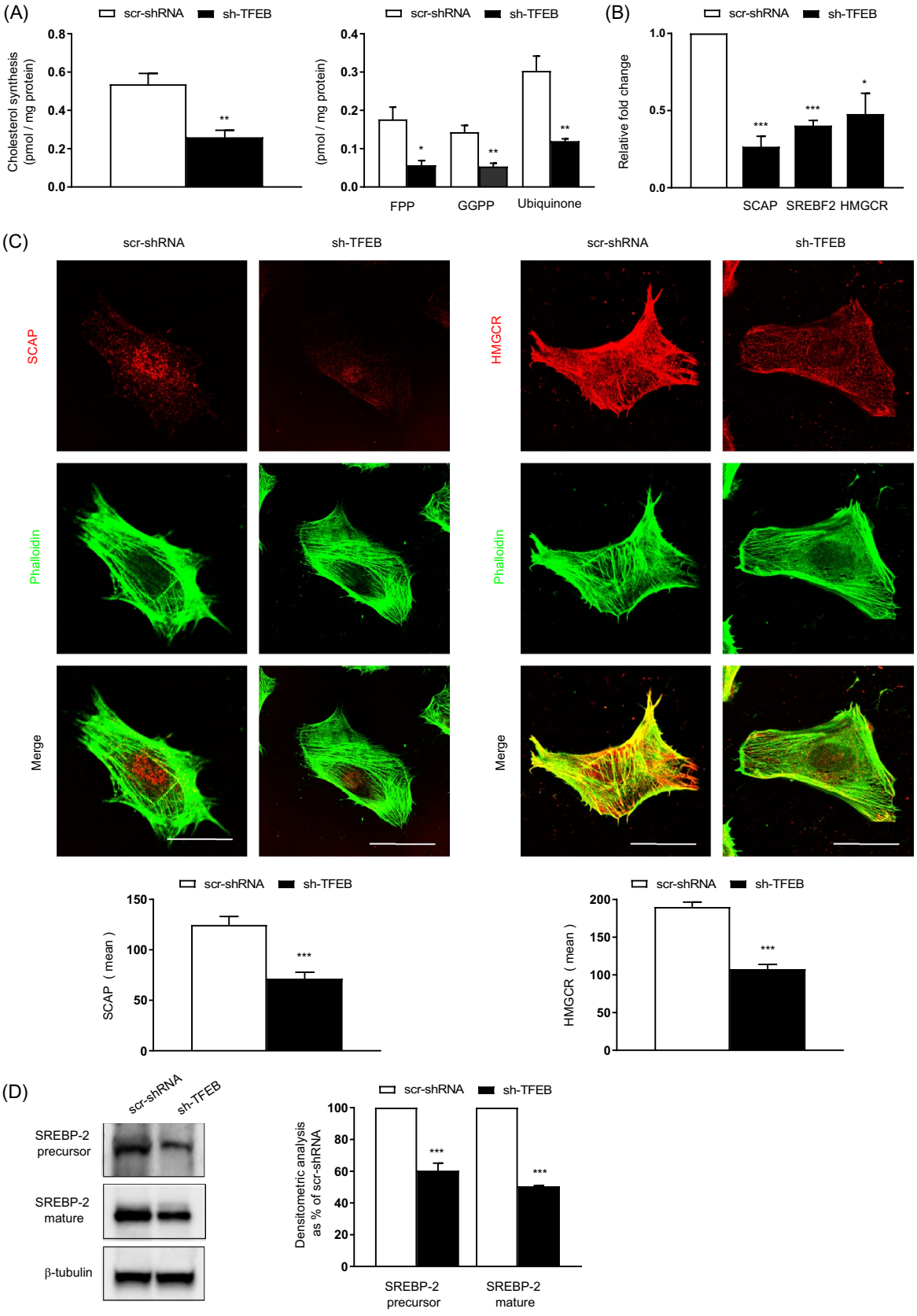
(A)
scr-shRNA
sh-TFEB
Cholesterol synthesis (pmol / mg protein)
0.8
0.6
0.4
0.2
0.0
**
scr-shRNA
sh-TFEB
(pmol / mg protein)
0.4
0.3
0.2
0.1
0.0
*
**
**
FPP
GGPP
Ubiquinone
(B)
scr-shRNA
sh-TFEB
Relative fold change
1.0
0.5
0.0
***
***
*
SCAP
SREBF2
HMGCR
(C)
scr-shRNA
sh-TFEB
scr-shRNA
sh-TFEB
SCAP
HMGCR
Phalloidin
Phalloidin
Merge
Merge
scr-shRNA
sh-TFEB
SCAP (mean)
150
100
50
0
***
scr-shRNA
sh-TFEB
HMGCR (mean)
200
150
100
50
0
***
(D)
scr-shRNA
sh-TFEB
SREBP-2 precursor
SREBP-2 mature
β-tubulin
scr-shRNA
sh-TFEB
Densitometric analysis as % of scr-shRNA
100
80
60
40
20
0
***
***
SREBP-2 precursor
SREBP-2 mature

◂**Fig. 6** TFEB silencing inhibits cholesterol synthesis. **A** The bar graphs show the quantification of de novo cholesterol, FPP, GGPP and ubiquinone synthesis in scr-shRNA- and sh-TFEB-ECs grown in medium containing [3H] acetate ($n=3$ independent experiments; values as mean ± SEM; ***$p<0.0001$, **$p<0.001$ and *$p<0.01$ for sh-TFEB-ECs versus scr-shRNA-ECs, as determined by Student's *t* test). **B** qPCR of *SCAP, SREBF-2* and *HMGCR* expression in scr-shRNA- and sh-TFEB-ECs. The data are expressed as the relative fold changes in sh-TFEB-ECs compared with the expression in scr-shRNA-ECs after normalization to the housekeeping gene *TBP* ($n=3$ independent experiments; values as mean ± SEM; ***$p<0.0001$ and *$p<0.01$ for sh-TFEB-ECs *versus* scr-shRNA-ECs, as determined by Student's *t* test). **C** Confocal microscopy analysis of SCAP and HMGCR expression in scr-shRNA- and sh-TFEB-ECs stained with anti-SCAP or anti-HMGCR antibodies and phalloidin-488 (scale bar: 25 µm). The bar graph shows the quantification of the mean intensity of SCAP or HMGCR ($n=20$ cells per condition pooled from three independent experiments; values as mean ± SEM; ***$p<0.0001$ for sh-TFEB-ECs *versus* scr-shRNA-ECs, as determined by Student's *t* test). **D** Representative western blots of the cellular amounts of unprocessed or mature SREBP2 expression in scr-shRNA- and sh-TFEB-ECs. The bar graph shows the densitometric results expressed as the ratio of SREBP2 to β-tubulin ($n=3$ independent experiments; mean ± SEM; ***$p<0.0001$ for sh-TFEB-ECs *versus* scr-shRNA-ECs, as determined by Student's *t* test)

and the ensuing polymerization of new FN [71]. On the contrary, CDC42, which favors PGC-based secretion, opposes RHOJ inhibition of FN fibrillogenesis [71]. In ECs Syntaxin-6 mediates α5β1 integrin recycling while its inhibition sustains the increase of α5 ubiquitination and α5β1 lysosome-dependent degradation [72]. Finally, ECs treatment with macrophage-derived exosomes increases the ubiquitination of integrin β1, its internalization and lysosomal degradation [73].

Interestingly, TFEB regulates the expression of several master genes involved in vesicular trafficking [23–25]. This function supports the observation in pancreatic ductal adenocarcinoma that TFEB promotes the endocytosis of α5β1 integrin and the disassembly focal adhesion by modulating RAB5 and in hepatocellular carcinoma the degradation of β1 integrin by activating lysosome machinery [74, 75].

Altogether these data indicate that TFEB controls integrin endocytosis by a cholesterol-mediate regulation of the caveolin machinery. However, in our experimental conditions we cannot exclude a minor role of clathrin-dependent endocytosis, despite the addition of exogenous cholesterol largely rescued the phenotype changes observed in sh-TFEB-ECs. However, this point requires further investigations. Actually, cholesterol is also involved in clathrin-dependent endocytosis. It has been reported that sterol-dependent membrane properties influence this endocytic mechanism [76], which is blocked by the acute depletion of cholesterol [77].

Our experiments demonstrate that TFEB silencing lead to the increase of ECs adhesion concomitant to a dynamic modification of FAs and FBs supported by elevated amount of integrin on plasma membrane via the regulation of cholesterol synthesis and lysosomal-dependent degradation. Actually, the sh-TFEB-ECs phenotype differs from that observed in other cellular types in which only cholesterol level or integrin recycling was modified while integrin lysosomal degradation was unchanged. In sarcoma cells that express high level of α5β1 integrin the modification of cholesterol level induces changes in cell shape, the inhibition of adhesion and migration on FN [78]. These alterations are connected with cholesterol regulation of actin cytoskeleton remodeling without any significant alteration of integrin behavior [78]. In Chinese hamster ovary cells (CHO-cells) the alteration of cholesterol at Trans-Golgi/endosome boundaries leads to Syntaxin-6 increase into recycling endosomes influencing the recycling of αvβ3 and α5β1 integrins [79]. Moreover, the same cells overexpressing Annexin 6 are characterized by the inhibition of late endosome cholesterol export and Syntaxin-6 mis-localization that summarize with a reduced cell surface integrin amount [80].

In conclusion, we show how the oncogenic transcription factor TFEB has a relevant impact on the regulation of vascular EC adhesion to the ECM through multiple mechanisms. In particular, beyond its canonical function in lysosome genesis and receptor degradation, TFEB can impact integrin-mediated EC adhesion through the regulation of integrin internalization and trafficking, and these effects are exerted through the metabolic control of endogenous cholesterol synthesis and CAV-1 pro-endocytic function.

Materials and methods

Reagents

The following reagents were used in this study: High-Capacity cDNA Reverse Transcription kit, TaqMan PCR Universal Master Mix, TaqMan assays, EZ-Link™ Sulfo-NHS-SS-Biotin, MaxiSorp 96-well plates, phalloidin, DAPI and TO-PRO-3-Stain obtained from Thermo Fisher Scientific; streptavidin-agarose beads obtained from Upstate Biotechnology; [^{3}H]-acetate (3600 mCi/mmol) purchased from Amersham Bioscience (Little Chalfont, UK); fluorometric Cholesterol/ Cholesteryl Ester Assay Kit—Quantitation was obtained from Abcam (Cambridge, UK); and [^{3}H]-cholesterol (7 Ci/mmol) procured from PerkinElmer (Walthman, MA); Empty Columns PD-10 and Gelatin Sepharose 4B (GE Healthcare).

All other reagents were obtained from Merck KGaA.

Antibodies

The following antibodies were used in this study: anti-integrin β1 (JB1B) (Abcam); anti-β1 integrin, anti-LAMP1, anti-Integrin alpha5 antibody (SNAKA-51) and phalloidin-Atto

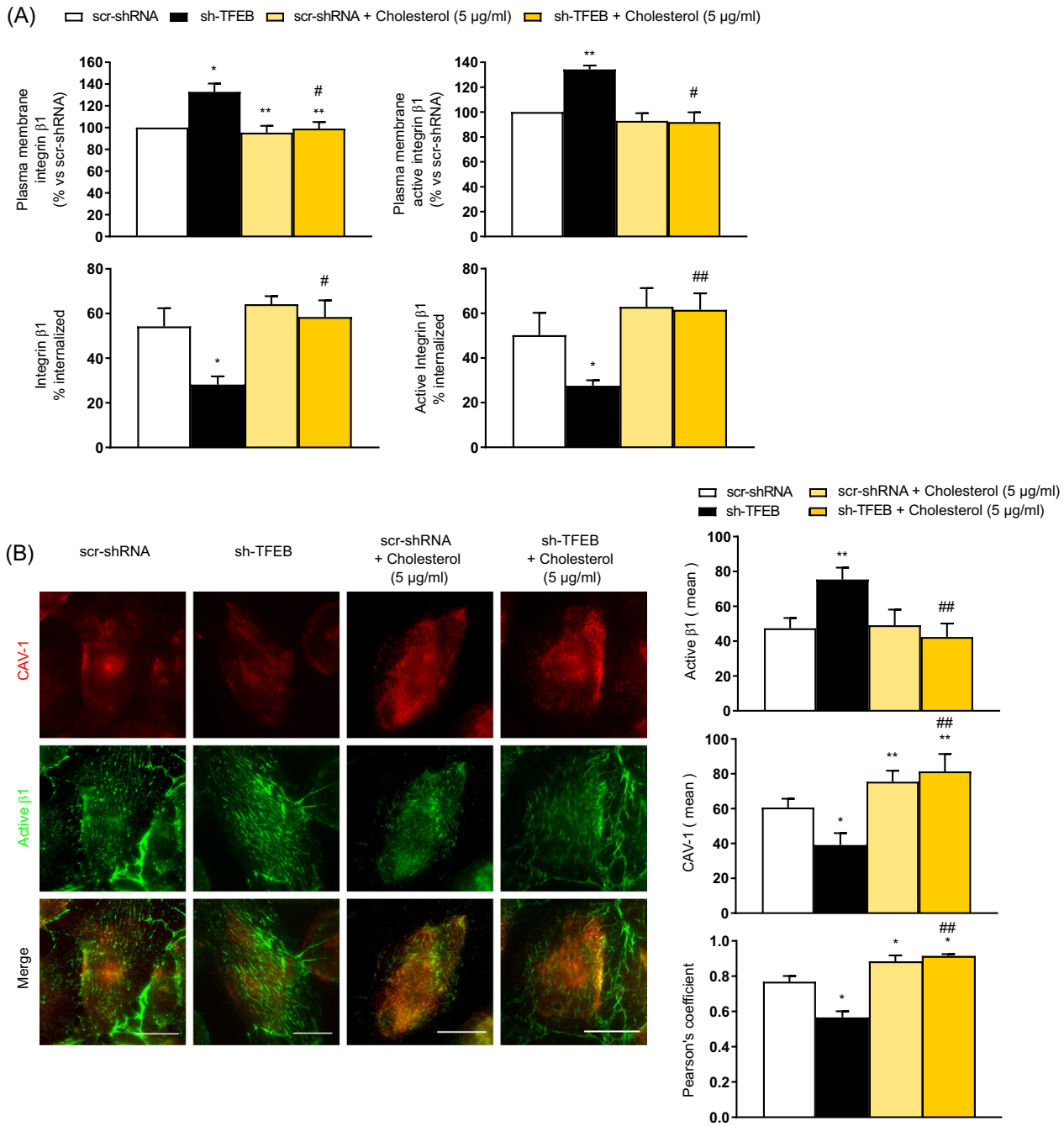

Fig. 7 Exogenous cholesterol abrogates TFEB silencing effects on integrin and CAV-1 membrane distribution. **A** Analysis of the relative amounts of internalized total and active β1 integrin in scr-shRNA-ECs and sh-TFEB-ECs supplemented or not supplemented with cholesterol (5 µg/ml, 24 h). Integrin internalization (after 30 min of induction) was evaluated by integrin internalization assay and capture ELISA assay ($n=3$ independent experiments, values as mean ± SEM, $^{**}p<0.001$, $^{*}p<0.01$ all samples *versus* scr-shRNA-ECs by Student's *t* test; $^{\#\#}p<0.001$ and $^{\#}p<0.01$ for sh-TFEB-ECs supplemented with cholesterol *versus* sh-TFEB-ECs, as determined by Student's *t* test). **B** Representative TIRF images of active β1 integrin and CAV-1 in living scr-shRNA- and sh-TFEB-ECs supplemented or not supplemented with cholesterol (5 µg/ml, 24 h). After in vivo incubation with anti-active β1 integrin (9EG7) antibody, cells were stained with anti-CAV-1 antibody (scale bar: 25 µm). The bar graphs show the quantification of the mean intensity of active β1 integrin and CAV-1 and the proximity of the two proteins analyzed with Pearson's coefficient ($n=20$ cells per condition pooled from three independent experiments; values as mean ± SEM; $^{**}p<0.001$ and $^{*}p<0.01$ for all samples *versus* scr-shRNA-ECs, as determined by Student's *t*-test; $^{\#\#}p<0.001$ for sh-TFEB-ECs supplemented with cholesterol *versus* sh-TFEB-ECs, as determined by Student's *t*-test).

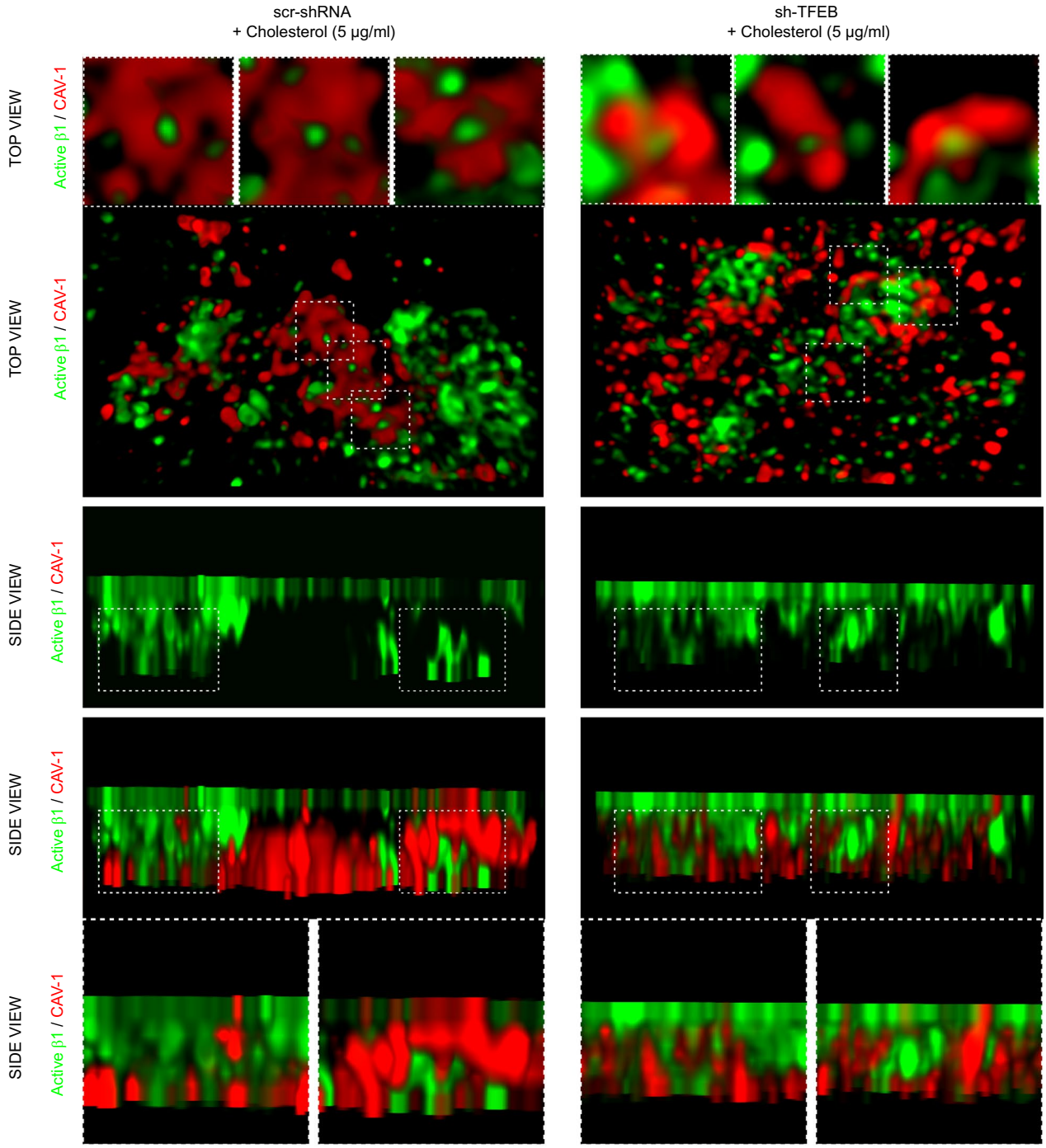

Fig. 8 Exogenous cholesterol rescues TFEB silencing inhibition of integrin internalization. Representative 3D-STED super-resolution image of active β1 integrin and CAV-1 expression and localization in living scr-shRNA- and sh-TFEB-ECs supplemented with cholesterol (5 µg/ml, 24 h). After in vivo incubation with anti-active β1 integrin (9EG7) antibody, cells were stained with anti-CAV-1 antibody (scale bar: 0.5 µm; $n=5$ cells per condition pooled from three independent experiments)

(Merck KGaA); anti-β-tubulin, anti-paxillin (5H11), SCAP, SREBP2, HMGCR, Alexa Fluor-tagged secondary antibody (Thermo Fisher Scientific); anti-active CD29 (9EG7) (BD Biosciences); anti-TFEB (MyBioSource); anti-CAV-1 and Mouse Mab anti-ED-A Fibronectin (ED-A FN) IST-9 (Santa Cruz Biotechnology); peroxidase-conjugated AffiniPure Rabbit-anti-Goat-IgG, Goat-anti-Mouse IgG and Goat-anti-Rabbit IgG (Jackson ImmunoResearch Laboratories).

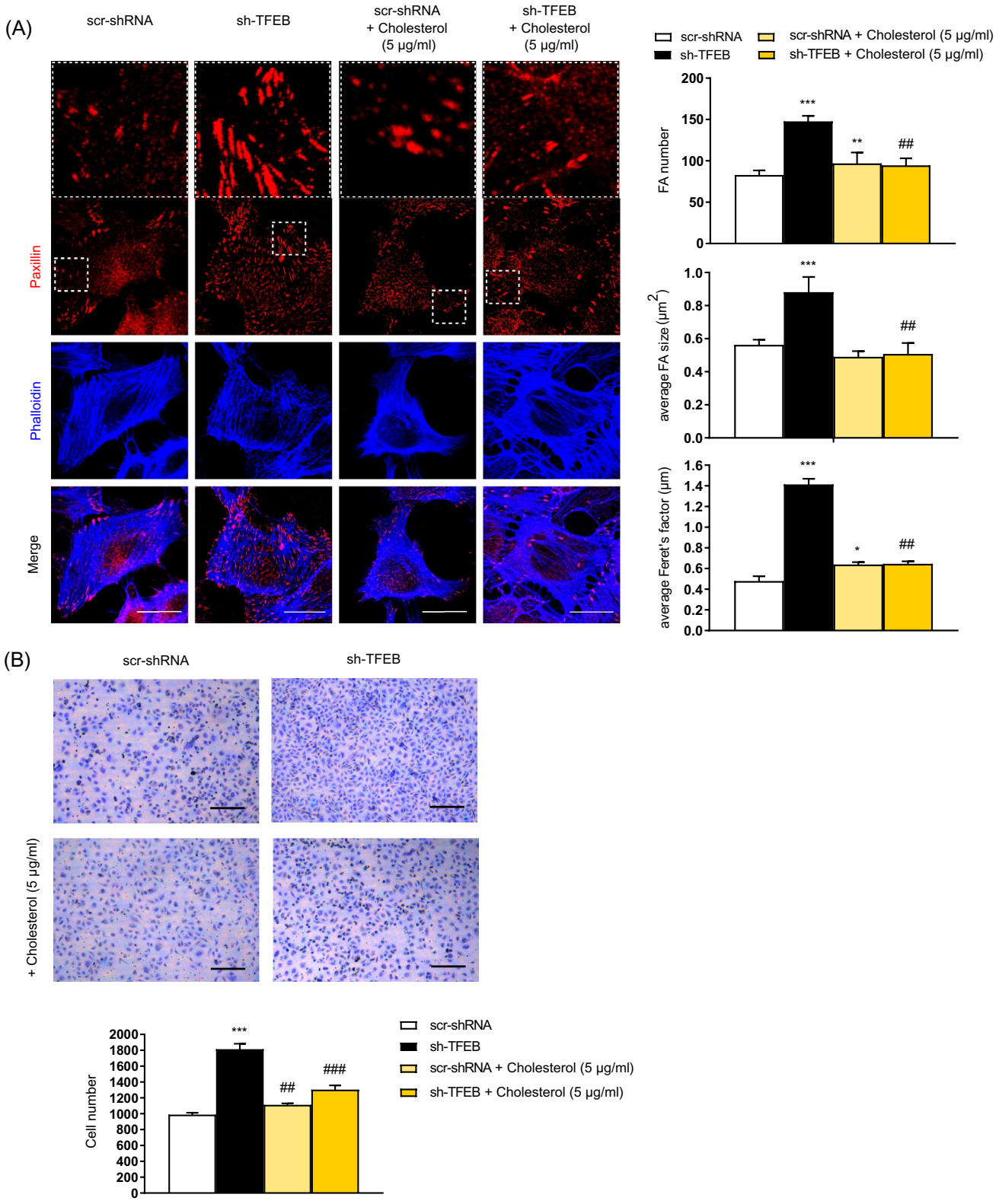

Cells and genetic manipulation

The experiments were performed using human endothelial cells (HUVECs) isolated from umbilical-cord veins maintained as described previously [25]. To minimize cell variability, pools of five different donors were used [81]. The isolation of primary HUVECs was approved by the Office of the General Director and Ethics Committee of the Azienda

◂**Fig. 9** Exogenous cholesterol rescues TFEB silencing effects on FAs development and ECs adhesion. **A** Confocal microscopy analysis of scr-shRNA- and sh-TFEB-ECs supplemented or not supplemented with cholesterol (5 µg/ml, 24 h) stained with anti-paxillin Ab and phalloidin-647 (scale bar: 25 µm). The bar graphs show the quantification of the FA number, the average FA area and the average Feret's diameter ($n=20$ cells per condition pooled from three independent experiments; values as mean ± SEM; $^{***}p<0.0001$, $^{**}p<0.001$ and $^{*}p<0.001$ for all samples *versus* scr-shRNA-ECs, as determined by Student's *t* test; $^{\#\#}p<0.001$ for sh-TFEB-ECs supplemented with cholesterol *versus* sh-TFEB-ECs, as determined by Student's *t* test). **B** Representative images of adherent scr-shRNA- and sh-TFEB-ECs supplemented or not supplemented with cholesterol (5 µg/ml, 24 h) seeded on FN (10× magnification, scale bar: 200 µm). The numbers of adherent cells are plotted as the mean ± SEM ($n=3$ independent experiments; $^{***}p<0.0001$ for sh-TFEB-ECs *versus* scr-shRNA-ECs, as determined by Student's *t* test; $^{\#\#\#}p<0.0001$ and $^{\#\#}p<0.001$ for sh-TFEB-ECs supplemented with cholesterol *versus* sh-TFEB-ECs, as determined by Student's *t* test)

Sanitaria Ospedaliera Ordine Mauriziano of Torino Hospital (protocol approval no. 586, Oct 22 2012 and no. 26884, Aug 28 2014, no. 1494 July 9 2018 and no. 0005355 May 03 2021), and informed consent was obtained from each patient. The cells were tested for mycoplasma contamination using a Venor GeM Mycoplasma Detection kit.

Loss-of-function experiments were performed with scramble control shRNA or shRNA against TFEB (shRNA #1: TRCN0000013111, shRNA #2: TRCN0000013110 and shRNA #3: TRCN0000437246 NM_007162.2) cloned in the pLKO.1-puro non-Mammalian vector. These cells were named scr-shRNA-ECs and sh-TFEB-ECs #1 or sh-TFEB-ECs #2 or sh-TFEB-ECs #3, respectively. We verified the efficiency, specificity and the putative off-targets effects of the different sh-RNAs against TFEB not finding any difference between them as shown in Fig S1. Since in previous works we had used the sh-RNA #1 [25] it was chosen again for the development of the entire study. HUVECs were transduced with specific lentiviral particles (MOI = 1) prepared according to Follenzi et al. [82]. The medium was replaced after 24 h, and cells stably expressing the lentivirus were selected on puromycin (1 µg/ml) for 24 h. As previously described [25], we verified the upregulation or inhibition of TFEB in ECs by qPCR, immunofluorescence and immunoblotting analyses.

SiRNA-mediated HMGCR silencing in ECs was performed by the use of RNAiMAX lipofectamine in Optimem medium according to the manufacturer's protocol. Loss-of-function experiments were performed with commercial scramble control siRNA negative control #1 or siRNA against HMGCR (60 nM, 24 h) (SASI_Hs01_00014353; SASI_Hs01_00014354; SASI_Hs01_00014355; SASI_Hs02_00303376). We verified the inhibition of HMGCR in ECs by qPCR and immunofluorescence analysis.

Adhesion assay

HUVECs (10×10^4 cells/well, six wells per condition) were seeded in 20% FBS medium in 96-well plates coated with fibronectin (3 µg/ml). After 2 h of incubation at 37 °C in the presence of 5% CO_2, the not-adherent cells were washed away with PBS, and the adherent cells were fixed in 2.5% glutaraldehyde for 30 min and stained with 0.1% crystal violet. Four random fields of each sample were counted at 10× magnification.

Integrin recycling assay

Integrin internalization assays were performed as previously described [36]. HUVECs were PM-labeled at 4 °C with 0.5 mg/ml sulfo-NHS-SS-biotin in PBS for 30 min on ice. The labeled cells were washed with cold MEM with 1% FBS and cold PBS, and endocytosis was induced with prewarmed MEM, 1% FBS. At the indicated times, the cells were transferred to ice, and biotin was removed from the plasma membrane by incubation with 20 mM sodium 2-mercaptoethanesulfonate (MesNa) in 50 mM Tris–HCl (pH 8.6), 100 mM NaCl, and 0.015 N NaOH for 1 h at 4 °C. MesNa was quenched by the addition of 20 mM iodoacetamide for 10 min. To measure integrin degradation in ECs we induced internalization as previously described and then cells were lysed after the different times. The cells were lysed in a specific buffer (25 mM Tris–HCl, pH 7.6, 100 mM NaCl, 2 mM $MgCl_2$, 1 mM Na_3VO_4, 0.5 mM EGTA, 1% Triton X-100, 5% glycerol, and protease and phosphatase inhibitor cocktail) at 4 °C. The lysates were cleared by centrifugation at 12,000 g for 20 min, and the levels of biotinylated integrin were determined by capture-ELISA.

Capture ELISA

Corning 96-well Clear Polystyrene High Bind Stripwell Microplates were coated overnight with 5 µg/ml specific anti-integrin antibodies in 0.05 M Na_2CO_3 (pH 9.6) at 4 °C and then blocked in PBS containing 0.05% Tween-20 with 5% BSA for 1 h at RT.

Integrins were captured by overnight incubation of 50 µl of cell lysate at 4 °C. The unbound material was removed by washing with PBS-Tween. Biotin-integrin complexes were bound with streptavidin-conjugated horseradish peroxidase in PBS-Tween with 1% BSA for 1 h at 4 °C and detected through a chromogenic reaction with ortho-phenylenediamine. The percentage of integrin internalization was calculated as the percentage of biotin-integrin complexes in cell lysates after internalization stimulation with respect to all the biotin-integrin complexes in unstimulated cells.

Quantification of immunofluorescence analysis

The cells were plated on 0.17-mm glass coverslips (no. 1.5) coated with fibronectin (3 µg/ml), in PBS and allowed to adhere overnight. The cells were washed in PBS, fixed in 4% PFA, permeabilized in 0.1% Triton X-100 for 8 min at 4 °C or with 0,1% saponin in PBS for 5 min at 4 °C, saturated with 1% donkey serum in PBS (30 min) and incubated with specific primary antibodies for 1 h at RT and then with appropriate Alexa Fluor-tagged secondary antibodies.

For evaluation of the plasma membrane integrin amount and fibrillogenesis, living cells on coverslips were incubated with anti-β1 integrin (JB1B), anti-active β1 integrin (9EG7) anti-anti-active α5β1 integrin (SNAKA-51) antibodies labeling the extracellular domain of the protein for 20 min at 37 °C, washed with PBS, fixed, permeabilized, stained with Alexa Fluor antibody and then processed for immunofluorescence detection.

A Leica TCS SP8 gated stimulated emission depletion (g-STED) 3 × laser-scanning microscope was used to acquire super-resolved images (Leica Microsystems). Different fields (5–8) from each sample section were randomly chosen for analysis. When evaluating the same molecule in different samples, the laser power, gain and offset settings were maintained. The images were quantified using ImageJ software.

The integrin amount in lysosomes, early endosomes was analyzed using ImageJ by creating a mask around the LAMP-1 + , EEA1 + or CAV-1 + vesicles and measuring the mean intensity of integrin in the area identified by the mask. The inhibition of endosome acidification was performed by the incubation of ECs with bafilomycin A1 (30 nM, 24 h).

For quantification of the FA and fibrillar adhesion number, area and Feret's factor, all the images were thresholded using an empirically determined value that was selected to better identify adhesive structures and exclude nonspecific noise. This value was maintained constant for all the images obtained with the different conditions and experiments. Using the ImageJ shape descriptor aspect ratio (AR), we identified the paxillin-positive objects by selecting only those that displayed a major-to-minor axis ratio < 5 per 100 µm^2 of cell area, whereas for fibrillar adhesions, we identified the anti-active β1 integrin (9EG7)-positive objects based on a major-to-minor axis ratio ≥ 1 per 100 µm^2 of cell area.

TIRF microscopy was performed using a Leica AM TIRF MC system mounted on a Leica AF 6000LX workstation with a 63X oil-immersion objective and a laser penetration depth of 90 nm. ECs were incubated with anti-active β1 integrin (9EG7) antibodies for 20 min at 37 °C, were fixed, saturated and permeabilized, and then treated with Ab anti-CAV-1 and appropriate Alexa fluor secondary Ab.

FN fibrillogenesis

Cells were seeded in 6-well dishes at a concentration of 4×10^5 cells per well and left to adhere for 3 or 16 h medium containing FN-depleted serum were incubated with IST-9 antibody, washed with PBS, fixed with 4% PFA and processed for immunofluorescence. The amount of ED-A FN fibrils was quantified. FN-depleted FCS was prepared according to previously described protocol [35] by the use of gelatin-Sepharose 4B.

Real-time PCR

Extracted RNA was converted to cDNA using a High-Capacity cDNA Reverse Transcription kit. Real-time PCR was performed using a CFX96 system (Bio-Rad) with TaqMan PCR Universal Master Mix and specific TaqMan assays. The experiments were performed in triplicate, and *TBP* was used as a reference gene.

The following TaqMan assays were used: TFEB (Hs00292981_m1), ITGB1 s01127536_m1), ITGB3 (Hs01001469_m1), ITGA5 (Hs01547673_m1), ITGAV (Hs00233808_m1), CAV-1 (Hs00971716_m1), SCAP (Hs00378725_m1), SREBF-2 (Hs01081784_m1), HMGCR (Hs00168352_m1), and TBP (Hs00427620).

Western blot

Western blotting and quantitative analysis were performed using the specific above-mentioned antibodies, a ChemiDoc Touch Imaging System (Bio-Rad) and Image Lab software 5.2.1 (Bio-Rad) as previously described [25].

Immunoprecipitation

Cells were washed with cold PBS and lysed in buffer with added protease and phosphatase inhibitors (50 µg/ml pepstatin, 50 µg/ml leupeptin, 10 µg/ml aprotinin, 1 mM phenylmethylsulfonyl fluoride, 100 µM $ZnCl_2$, 1 mM Na_3VO_4). To immunoprecipitate integrin complexes, a buffer containing 50 mM HEPES (pH 7.4), 5 mM EDTA, 2 mM EGTA, 150 mM NaCl, 10% glycerol, and 1% NP-40 was used. For all of the other conditions of immunoprecipitation, a buffer containing 10 mM Tris–HCl pH 7.5, 150 mM NaCl, 5 mM EDTA, 1% Triton X-100, 10% glycerol was used. Lysates (1 mg) were precleared for 2 h at 4 °C and then incubated with protein G-Sepharose or protein A-Sepharose and anti-active β1 integrin (9EG7) or active α5β1 integrin (SNAKA-51) or anti-β1 integrin antibodies for 2 h at 4 °C. After resuspension in 50 mM Tris–HCl pH 7.4, 2% SDS and heated for 5 min at 95 °C, immunoprecipitates were resolved by SDS-PAGE and immunoblotted as indicated. In the same lysates used for immunoprecipitation, the endogenous expression of

total β1 integrin and β-tubulin were blotted with the specific antibody and presented as "input".

De novo synthesis of isoprenoids and cholesterol

Cells (0.5×10^6) were grown in medium containing 10% FBS, radiolabeled with 1 μCi [^{3}H]-acetate for 24 h and then washed twice with PBS. A 50-μl aliquot was sonicated and used to measure the protein content, and the remaining cell suspension was subjected to 1:2 methanol/hexane lysis for the collection of lipid species. Lipids resuspended in 30 μl of chloroform were separated by thin layer chromatography (TLC) using a 1:1 (v/v) ether/hexane solution as the mobile phase and LK6DWhatman silica gels (Merck, Darmstadt, Germany). Solutions of 10 mg/ml cholesterol, ubiquinone, FPP or GPP were used as standards. The silica gel plates were exposed for 1 h to an iodine-saturated atmosphere, the migrated spots were cut out, and their radioactivity was measured by liquid scintillation using a Tri-Carb Liquid Scintillation Analyzer (PerkinElmer, Waltham, MA, USA) [83]. The results were determined using previously prepared calibration curves and are expressed as pmoles/mg cellular proteins.

Free cholesterol quantification

The fluorometric Cholesterol/Cholesteryl Ester Assay Kit—Quantitation was used to measure the level of free cholesterol in cell lysates in accordance to the manufacturer's instructions. The results are expressed as mg cholesterol or cholesteryl esters/mg cellular proteins.

Cholesterol uptake and efflux

Cells (0.5×10^6) were grown in medium containing 10% FBS and radiolabeled with 1 μCi [^{3}H]-cholesterol (7 Ci/mmol). In the uptake assay, the medium was removed after 0.5 h, and the cells were washed five times with PBS and detached. The radioactivity of the cell suspension, which is a measure of cholesterol uptake, was measured by liquid scintillation. In the efflux assay, the medium was removed after 1 h, and the cells were washed five times with PBS and allowed to grow for an additional 24 h. After this incubation time, the extracellular medium was collected, and the radioactivity, which serves as an index of cholesterol efflux over 24 h, was determined by liquid scintillation [83]. The count per minute (cpm) of scr-shRNA-ECs-treated cells was considered 100%, and the results are expressed as the percentages of the cpm of the experimental cells versus that of the scr-shRNA-treated ECs.

Statistical analysis

The sample sizes were not selected according to a specific power analysis but were consistent with those used in similar experiments performed in other laboratories investigating vascular development and quoted in the specific references. No statistical methods were used to predetermine the sample size. We did not randomize the samples because our experimental design did not require this type of strategy. The investigators were not blinded to the allocation of the samples during the experiments and analyses. The data are presented as the mean ± SEM.

The statistical analyses were performed using Excel (Microsoft) and Prism (GraphPad) software. Appropriate statistical tests were performed as indicated in the Results section, and $p < 0.05$ was considered to indicate statistical significance in all the experiments.

Supplementary Information The online version contains supplementary material available at https://doi.org/10.1007/s10456-022-09840-x.

Acknowledgements This work was supported by AIRC—Associazione Italiana per la Ricerca sul Cancro (grants 22910, 12182 and 18652), Regione Piemonte (Grant A1907A, Deflect), Fondazione CRT, Ministero dell'Università e della Ricerca (PRIN 2017, Grant 2017237P5X), FPRC 5xmille 2016 MIUR (Biofilm) and ERA-Net Transcan-2 (Grant TRS-2018-00000689) to FB.

Author contributions Conceptualization, GD, FB, DC, GS, CR; Methodology, GD, DC, GM, CA, DV; Formal Analysis, GD,DC; Investigation, GD, DC, GM, DV, EA, CR; Resources, FB; Writing-Original Draft, GD, FB, GS; Writing-Review & Editing, GD, FB, GS; Supervision, FB; Funding acquisition, FB.

Funding Open access funding provided by Università degli Studi di Torino within the CRUI-CARE Agreement.

Declarations

Conflict of interest The authors declare no competing interests.

References

1. Bussolino F, Mantovani A, Persico G (1997) Molecular mechanisms of blood vessel formation. Trends Biochem Sci 22:251–256
2. Korn C, Augustin HG (2015) Mechanisms of vessel pruning and regression. Dev Cell 34:5–17
3. Avraamides CJ, Garmy-Susini B, Varner JA (2008) Integrins in angiogenesis and lymphangiogenesis. Nat Rev Cancer 8:604–617
4. Weis SM, Cheresh DA (2011) Tumor angiogenesis: molecular pathways and therapeutic targets. Nat Med 17:1359–1370
5. Mana G, Valdembri D, Serini G (2020) Conformationally active integrin endocytosis and traffic: why, where, when and how? Biochem Soc Trans 48:83–93
6. Moreno-Layseca P, Icha J, Hamidi H, Ivaska J (2019) Integrin trafficking in cells and tissues. Nat Cell Biol 21:122–132
7. Parton RG (2018) Caveolae: structure, function, and relationship to disease. Annu Rev Cell Dev Biol 34:111–136
8. Hayer A, Stoeber M, Bissig C, Helenius A (2010) Biogenesis of caveolae: stepwise assembly of large caveolin and cavin complexes. Traffic 11:361–382
9. Tagawa A, Mezzacasa A, Hayer A, Longatti A, Pelkmans L, Helenius A (2005) Assembly and trafficking of caveolar domains in the cell: caveolae as stable, cargo-triggered, vesicular transporters. J Cell Biol 170:769–779
10. Rothberg KG, Heuser JE, Donzell WC, Ying YS, Glenney JR, Anderson RG (1992) Caveolin, a protein component of caveolae membrane coats. Cell 68:673–682
11. Shi F, Sottile J (2008) Caveolin-1-dependent beta1 integrin endocytosis is a critical regulator of fibronectin turnover. J Cell Sci 121:2360–2371
12. Filippini A, Sica G, D'Alessio A (2018) The caveolar membrane system in endothelium: From cell signaling to vascular pathology. J Cell Biochem 119:5060–5071
13. Sowa G (2012) Caveolae, caveolins, cavins, and endothelial cell function: new insights. Front Physiol 2:120
14. Norman LL, Oetama RJ, Dembo M, Byfield F, Hammer DA, Levitan I, Aranda-Espinoza H (2010) Modification of cellular cholesterol content affects traction force, adhesion and cell spreading. Cell Mol Bioeng 3:151–162
15. Ao M, Wu L, Zhou X, Chen Y (2016) Methyl-β-cyclodextrin impairs the monocyte-adhering ability of endothelial cells by down-regulating adhesion molecules and caveolae and reorganizing the actin cytoskeleton. Biol Pharm Bull 39:1029–1034
16. Haq R, Fisher DE (2011) Biology and clinical relevance of the micropthalmia family of transcription factors in human cancer. J Clin Oncol 29:3474–3482
17. Medina DL, Fraldi A, Bouche V, Annunziata F, Mansueto G, Spampanato C, Puri C, Pignata A, Martina JA, Sardiello M, Palmieri M, Polishchuk R, Puertollano R, Ballabio A (2011) Transcriptional activation of lysosomal exocytosis promotes cellular clearance. Dev Cell 21:421–430
18. Napolitano G, Ballabio A (2016) TFEB at a glance. J Cell Sci 129:2475–2481
19. Palmieri M, Impey S, Kang H, di Ronza A, Pelz C, Sardiello M, Ballabio A (2011) Characterization of the CLEAR network reveals an integrated control of cellular clearance pathways. Hum Mol Genet 20:3852–3866
20. Sardiello M, Palmieri M, di Ronza A, Medina DL, Valenza M, Gennarino VA, Di Malta C, Donaudy F, Embrione V, Polishchuk RS, Banfi S, Parenti G, Cattaneo E, Ballabio A (2009) A gene network regulating lysosomal biogenesis and function. Science 325:473–477
21. Astanina E, Bussolino F, Doronzo G (2020) Multifaceted activities of transcription factor eb in cancer onset and progression. Mol Oncol 15:327–346
22. Corà D, Bussolino F, Doronzo G (2021) TFEB signalling-related MicroRNAs and autophagy. Biomolecules 11:985
23. Nnah IC, Wang B, Saqcena C, Weber GF, Bonder EM, Bagley D, De Cegli R, Napolitano G, Medina DL, Ballabio A, Dobrowolski R (2019) TFEB-driven endocytosis coordinates MTORC1 signaling and autophagy. Autophagy 15:151–164
24. Raben N, Puertollano R (2016) TFEB and TFE3: linking lysosomes to cellular adaptation to stress. Annu Rev Cell Dev Biol 32:255–278
25. Doronzo G, Astanina E, Corà D, Chiabotto G, Comunanza V, Noghero A, Neri F, Puliafito A, Primo L, Spampanato C, Settembre C, Ballabio A, Camussi G, Oliviero S, Bussolino F (2019) TFEB controls vascular development by regulating the proliferation of endothelial cells. EMBO J 38:e98250
26. Lu H, Fan Y, Qiao C, Liang W, Hu W, Zhu T, Zhang J, Chen YE (2017) TFEB inhibits endothelial cell inflammation and reduces atherosclerosis. Sci Signal 10:eaah4214
27. Fan Y, Lu H, Liang W, Garcia-Barrio MT, Guo Y, Zhang J, Zhu T, Hao Y, Chen YE (2018) Endothelial TFEB (transcription factor EB) positively regulates postischemic angiogenesis. Circ Res 122:945–957
28. Emanuel R, Sergin I, Bhattacharya S, Turner J, Epelman S, Settembre C, Diwan A, Ballabio A, Razani B (2014) Induction of lysosomal biogenesis in atherosclerotic macrophages can rescue lipid-induced lysosomal dysfunction and downstream sequelae. Arterioscler Thromb Vasc Biol 34:1942–1952
29. Steingrímsson E, Tessarollo L, Reid SW, Jenkins NA, Copeland NG (1998) The bHLH-Zip transcription factor Tfeb is essential for placental vascularization. Development 125:4607–4616
30. Cho CH, Lee CS, Chang M, Jang IH, Kim SJ, Hwang I, Ryu SH, Lee CO, Koh GY (2004) Localization of VEGFR-2 and PLD2 in endothelial caveolae is involved in VEGF-induced phosphorylation of MEK and ERK. Am J Physiol Heart Circ Physiol 286:H1881-1888
31. Labrecque L, Royal I, Surprenant DS, Patterson C, Gingras D, Béliveau R (2003) Regulation of vascular endothelial growth factor receptor-2 activity by caveolin-1 and plasma membrane cholesterol. Mol Biol Cell 14:334–347
32. Mettouchi A (2012) The role of extracellular matrix in vascular branching morphogenesis. Cell Adh Migr 6:528–534
33. Shapiro SD (1998) Matrix metalloproteinase degradation of extracellular matrix: biological consequences. Curr Opin Cell Biol 10:602–608
34. Schwarzbauer JE, DeSimone DW (2011) Fibronectins, their fibrillogenesis, and in vivo functions. Cold Spring Harb Perspect Biol 3:a005041
35. Clapero F, Tortarolo D, Valdembri D, Serini G (2021) Quantifying polarized extracellular matrix secretion in cultured endothelial cells. Methods Mol Biol 2217:301–311
36. Mana G, Clapero F, Panieri E, Panero V, Böttcher RT, Tseng HY, Saltarin F, Astanina E, Wolanska KI, Morgan MR, Humphries MJ, Santoro MM, Serini G, Valdembri D (2016) PPFIA1 drives active α5β1 integrin recycling and controls fibronectin fibrillogenesis and vascular morphogenesis. Nat Commun 7:13546
37. Valdembri D, Caswell PT, Anderson KI, Schwarz JP, Konig I, Astanina E, Caccavari F, Norman JC, Humphries MJ, Bussolino F, Serini G (2009) Neuropilin-1/GIPC1 signaling regulates alpha-5beta1 integrin traffic and function in endothelial cells. PLoS Biol 7:e25
38. Sottile J, Chandler J (2005) Fibronectin matrix turnover occurs through a caveolin-1-dependent process. Mol Biol Cell 16:757–768
39. De Franceschi N, Ivaska J (2015) Integrin bondage: filamin takes control. Nat Struct Mol Biol 22:355–357

40. Rosales C, O'Brien V, Kornberg L, Juliano R (1995) Signal transduction by cell adhesion receptors. Biochim Biophys Acta 1242:77–98
41. Burridge K, Turner CE, Romer LH (1992) Tyrosine phosphorylation of paxillin and pp125FAK accompanies cell adhesion to extracellular matrix: a role in cytoskeletal assembly. J Cell Biol 119:893–903
42. Hanks SK, Calalb MB, Harper MC, Patel SK (1992) Focal adhesion protein-tyrosine kinase phosphorylated in response to cell attachment to fibronectin. Proc Natl Acad Sci U S A 89:8487–8491
43. Rainero E, Norman JC (2013) Late endosomal and lysosomal trafficking during integrin-mediated cell migration and invasion: cell matrix receptors are trafficked through the late endosomal pathway in a way that dictates how cells migrate. BioEssays 35:523–532
44. Steinberg F, Heesom KJ, Bass MD, Cullen PJ (2012) SNX17 protects integrins from degradation by sorting between lysosomal and recycling pathways. J Cell Biol 197:219–230
45. Böttcher RT, Stremmel C, Meves A, Meyer H, Widmaier M, Tseng HY, Fässler R (2012) Sorting nexin 17 prevents lysosomal degradation of β1 integrins by binding to the β1-integrin tail. Nat Cell Biol 14:584–592
46. Brown MS, Radhakrishnan A, Goldstein JL (2018) Retrospective on cholesterol homeostasis: the central role of scap. Annu Rev Biochem 87:783–807
47. Yamamoto A, Tagawa Y, Yoshimori T, Moriyama Y, Masaki R, Tashiro Y (1998) Bafilomycin A1 prevents maturation of autophagic vacuoles by inhibiting fusion between autophagosomes and lysosomes in rat hepatoma cell line, H-4-II-E cells. Cell Struct Funct 23:33–42
48. Settembre C, De Cegli R, Mansueto G, Saha PK, Vetrini F, Visvikis O, Huynh T, Carissimo A, Palmer D, Klisch TJ, Wollenberg AC, Di Bernardo D, Chan L, Irazoqui JE, Ballabio A (2013) TFEB controls cellular lipid metabolism through a starvation-induced autoregulatory loop. Nat Cell Biol 15:647–658
49. Wang Y, Huang Y, Liu J, Zhang J, Xu M, You Z, Peng C, Gong Z, Liu W (2020) Acetyltransferase GCN5 regulates autophagy and lysosome biogenesis by targeting TFEB. EMBO Rep 21:e48335
50. Rainero E, Howe JD, Caswell PT, Jamieson NB, Anderson K, Critchley DR, Machesky L, Norman JC (2015) Ligand-occupied integrin internalization links nutrient signaling to invasive migration. Cell Rep 10:398–413
51. Georgiadou M, Ivaska J (2017) Tensins: bridging AMP-activated protein kinase with integrin activation. Trends Cell Biol 27:703–711
52. Georgiadou M, Lilja J, Jacquemet G, Guzmán C, Rafaeva M, Alibert C, Yan Y, Sahgal P, Lerche M, Manneville JB, Mäkelä TP, Ivaska J (2017) AMPK negatively regulates tensin-dependent integrin activity. J Cell Biol 216:1107–1121
53. Dornier E, Rabas N, Mitchell L, Novo D, Dhayade S, Marco S, Mackay G, Sumpton D, Pallares M, Nixon C, Blyth K, Macpherson IR, Rainero E, Norman JC (2017) Glutaminolysis drives membrane trafficking to promote invasiveness of breast cancer cells. Nat Commun 8:2255
54. Hardie DG, Ross FA, Hawley SA (2012) AMPK: a nutrient and energy sensor that maintains energy homeostasis. Nat Rev Mol Cell Biol 13:251–262
55. El-Houjeiri L, Possik E, Vijayaraghavan T, Paquette M, Martina JA, Kazan JM, Ma EH, Jones R, Blanchette P, Puertollano R, Pause A (2019) The transcription factors TFEB and TFE3 Link the FLCN-AMPK signaling axis to innate immune response and pathogen resistance. Cell Rep 26:3613–3628
56. Young NP, Kamireddy A, Van Nostrand JL, Eichner LJ, Shokhirev MN, Dayn Y, Shaw RJ (2016) AMPK governs lineage specification through Tfeb-dependent regulation of lysosomes. Genes Dev 30:535–552
57. Pastore N, Brady OA, Diab HI, Martina JA, Sun L, Huynh T, Lim JA, Zare H, Raben N, Ballabio A, Puertollano R (2016) TFEB and TFE3 cooperate in the regulation of the innate immune response in activated macrophages. Autophagy 12:1240–1258
58. Davis GE, Senger DR (2005) Endothelial extracellular matrix: biosynthesis, remodeling, and functions during vascular morphogenesis and neovessel stabilization. Circ Res 97:1093–1107
59. Noghero A, Perino A, Seano G, Saglio E, Lo Sasso G, Veglio F, Primo L, Hirsch E, Bussolino F, Morello F (2012) Liver X receptor activation reduces angiogenesis by impairing lipid raft localization and signaling of vascular endothelial growth factor receptor-2. Arterioscler Thromb Vasc Biol 32:2280–2288
60. Filippini A, D'Alessio A (2020) Caveolae and lipid rafts in endothelium: valuable organelles for multiple functions. Biomolecules 10:1218
61. Xu J, Dang Y, Ren YR, Liu JO (2010) Cholesterol trafficking is required for mTOR activation in endothelial cells. Proc Natl Acad Sci U S A 107:4764–4769
62. Shim JS, Li RJ, Lv J, Head SA, Yang EJ, Liu JO (2015) Inhibition of angiogenesis by selective estrogen receptor modulators through blockade of cholesterol trafficking rather than estrogen receptor antagonism. Cancer 362:106–115
63. Caliceti C, Zambonin L, Rizzo B, Fiorentini D, Vieceli Dalla Sega F, Hrelia S, Prata C (2014) Role of plasma membrane caveolae/lipid rafts in VEGF-induced redox signaling in human leukemia cells. Biomed Res Int 2014:857504
64. Santibanez JF, Blanco FJ, Garrido-Martin EM, Sanz-Rodriguez F, del Pozo MA, Bernabeu C (2008) Caveolin-1 interacts and cooperates with the transforming growth factor-beta type I receptor ALK1 in endothelial caveolae. Cardiovasc Res 77:791–799
65. Margadant C, Monsuur HN, Norman JC, Sonnenberg A (2011) Mechanisms of integrin activation and trafficking. Curr Opin Cell Biol 23:607–614
66. Lobert VH, Brech A, Pedersen NM, Wesche J, Oppelt A, Malerød L, Stenmark H (2010) Ubiquitination of alpha 5 beta 1 integrin controls fibroblast migration through lysosomal degradation of fibronectin-integrin complexes. Dev Cell 19:148–159
67. Kharitidi D, Apaja PM, Manteghi S, Suzuki K, Malitskaya E, Roldan A, Gingras MC, Takagi J, Lukacs GL, Pause A (2015) Interplay of endosomal pH and ligand occupancy in integrin α5β1 ubiquitination, endocytic sorting, and cell migration. Cell Rep 13:599–609
68. Dozynkiewicz MA, Jamieson NB, Macpherson I, Grindlay J, van den Berghe PV, von Thun A, Morton JP, Gourley C, Timpson P, Nixon C, McKay CJ, Carter R, Strachan D, Anderson K, Sansom OJ, Caswell PT, Norman JC (2012) Rab25 and CLIC3 collaborate to promote integrin recycling from late endosomes/lysosomes and drive cancer progression. Dev Cell 22:131–145
69. Sung BH, Zhu X, Kaverina I, Weaver AM (2011) Cortactin controls cell motility and lamellipodial dynamics by regulating ECM secretion. Curr Biol 21:1460–1469
70. Pellinen T, Arjonen A, Vuoriluoto K, Kallio K, Fransen JA, Ivaska J (2006) Small GTPase Rab21 regulates cell adhesion and controls endosomal traffic of beta1-integrins. J Cell Biol 173:767–780
71. Sundararaman A, Fukushima Y, Norman JC, Uemura A, Mellor H (2020) RhoJ regulates α5β1 integrin trafficking to control fibronectin remodeling during angiogenesis. Curr Biol 30:2146–2155
72. Tiwari A, Jung JJ, Inamdar SM, Brown CO, Goel A, Choudhury A (2011) Endothelial cell migration on fibronectin is regulated by syntaxin 6-mediated alpha5beta1 integrin recycling. J Biol Chem 286:36749–36761

73. Lee HD, Kim YH, Kim DS (2014) Exosomes derived from human macrophages suppress endothelial cell migration by controlling integrin trafficking. Eur J Immunol 44:1156–1169
74. He R, Wang M, Zhao C, Shen M, Yu Y, He L, Zhao Y, Chen H, Shi X, Zhou M, Pan S, Liu Y, Guo X, Li X, Qin R (2019) TFEB-driven autophagy potentiates TGF-β induced migration in pancreatic cancer cells. J Exp Clin Cancer Res 38:340
75. Zhang C, Yang H, Pan L, Zhao G, Zhang R, Zhang T, Xiao Z, Tong Y, Zhang Y, Hu R, Pandol SJ, Han YP (2021) Hepatitis B virus X protein (HBx) suppresses transcription factor EB (TFEB) resulting in stabilization of integrin beta 1 (ITGB1) in hepatocellular carcinoma cells. Cancers (Basel) 13:1181
76. Kim JH, Singh A, Del Poeta M, Brown DA, London E (2017) The effect of sterol structure upon clathrin-mediated and clathrin-independent endocytosis. J Cell Sci 130:2682–2695
77. Anderson RH, Sochacki KA, Vuppula H, Scott BL, Bailey EM, Schultz MM, Kerkvliet JG, Taraska JW, Hoppe AD, Francis KR (2021) Sterols lower energetic barriers of membrane bending and fission necessary for efficient clathrin-mediated endocytosis. Cell Rep 37:110008
78. Ramprasad OG, Srinivas G, Rao KS, Joshi P, Thiery JP, Dufour S, Pande G (2007) Changes in cholesterol levels in the plasma membrane modulate cell signaling and regulate cell adhesion and migration on fibronectin. Cell Motil Cytoskeleton 64:199–216
79. Reverter M, Rentero C, Garcia-Melero A, Hoque M, Vilà de Muga S, Alvarez-Guaita A, Conway JR, Wood P, Cairns R, Lykopoulou L, Grinberg D, Vilageliu L, Bosch M, Heeren J, Blasi J, Timpson P, Pol A, Tebar F, Murray RZ, Grewal T, Enrich C (2014) Cholesterol regulates syntaxin 6 trafficking at trans-golgi network endosomal boundaries. Cell Rep 7:883–897
80. García-Melero A, Reverter M, Hoque M, Meneses-Salas E, Koese M, Conway JR, Johnsen CH, Alvarez-Guaita A, Morales-Paytuvi F, Elmaghrabi YA, Pol A, Tebar F, Murray RZ, Timpson P, Enrich C, Grewal T, Rentero C (2016) Annexin A6 and late endosomal cholesterol modulate integrin recycling and cell migration. J Biol Chem 291:1320–1335
81. Nowak-Sliwinska P, Alitalo K, Allen E, Anisimov A, Aplin AC, Auerbach R, Augustin HG, Bates DO, van Beijnum JR, Bender RHF, Bergers G, Bikfalvi A, Bischoff J, Böck BC, Brooks PC, Bussolino F, Cakir B, Carmeliet P, Castranova D, Cimpean AM, Cleaver O, Coukos G, Davis GE, De Palma M, Dimberg A, Dings RPM, Djonov V, Dudley AC, Dufton NP, Fendt SM, Ferrara N, Fruttiger M, Fukumura D, Ghesquière B, Gong Y, Griffin RJ, Harris AL, Hughes CCW, Hultgren NW, Iruela-Arispe ML, Irving M, Jain RK, Kalluri R, Kalucka J, Kerbel RS, Kitajewski J, Klaassen I, Kleinmann HK, Koolwijk P, Kuczynski E, Kwak BR, Marien K, Melero-Martin JM, Munn LL, Nicosia RF, Noel A, Nurro J, Olsson AK, Petrova TV, Pietras K, Pili R, Pollard JW, Post MJ, Quax PHA, Rabinovich GA, Raica M, Randi AM, Ribatti D, Ruegg C, Schlingemann RO, Schulte-Merker S, Smith LEH, Song JW, Stacker SA, Stalin J, Stratman AN, Van de Velde M, van Hinsbergh VWM, Vermeulen PB, Waltenberger J, Weinstein BM, Xin H, Yetkin-Arik B, Yla-Herttuala S, Yoder MC, Griffioen AW (2018) Consensus guidelines for the use and interpretation of angiogenesis assays. Angiogenesis 21:425–532
82. Follenzi A, Ailles LE, Bakovic S, Geuna M, Naldini L (2000) Gene transfer by lentiviral vectors is limited by nuclear translocation and rescued by HIV-1 pol sequences. Nat Genet 25:217–222
83. Campia I, Sala V, Kopecka J, Leo C, Mitro N, Costamagna C, Caruso D, Pescarmona G, Crepaldi T, Ghigo D, Bosia A, Riganti C (2012) Digoxin and ouabain induce the efflux of cholesterol via liver X receptor signalling and the synthesis of ATP in cardiomyocytes. Biochem J 447:301–311